

Hermite interpolation with retractions on manifolds

Axel Séguin*

Daniel Kressner*

Abstract

Interpolation of data on non-Euclidean spaces is an active research area fostered by its numerous applications. This work considers the Hermite interpolation problem: finding a sufficiently smooth manifold curve that interpolates a collection of data points on a Riemannian manifold while matching a prescribed derivative at each point. A novel procedure relying on the general concept of retractions is proposed to solve this problem on a large class of manifolds, including those for which computing the Riemannian exponential or logarithmic maps is not straightforward, such as the manifold of fixed-rank matrices. The well-posedness of the method is analyzed by introducing and showing the existence of retraction-convex sets, a generalization of geodesically convex sets. A classical result on the asymptotic interpolation error of Hermite interpolation is extended to the manifold setting. Finally numerical experiments on the manifold of fixed-rank matrices and the Stiefel manifold of matrices with orthonormal columns illustrate these results and the effectiveness of the method.

1 Introduction

Data processing on non-Euclidean spaces has become a well-established tool in many fields of science and engineering. In particular, there has been a rising interest to interpolate data on a manifold with a curve contained in the manifold. This is motivated by numerous applications in robotics [PR95] [BCC21], computer vision [BKSL17], medical imaging [GSA14] [KDLS21], statistics [MMH⁺22] and model-order reduction [Ams10], just to mention a few. For example, motion-planning of a robotic manipulator can be carried out by interpolating points on the Lie group of rigid motions $SE(3)$ [PR95]. In statistical modeling, estimating covariance matrices between discrete samples of a random field can be viewed as interpolation on the manifold of symmetric positive definite matrices [MMH⁺22]. Reduced-order modeling in engineering typically involves projecting high-dimensional dynamics onto low-dimensional subspaces and interpolating such subspaces on the Grassman manifold is an important task for parameter-dependent systems [Ams10].

Over the last two decades, several ways of performing manifold interpolation computationally have been proposed. These methods are tailored to meet different requirements of the application, concerning the regularity of the interpolating curve and the nature of the interpolation constraints. In this present work, we focus on continuously differentiable interpolation curves that match prescribed data *and* velocities at each point; this is commonly known as *Hermite interpolation*.

*École Polytechnique Fédérale de Lausanne (EPFL) Institute of Mathematics, CH-1015 Lausanne, Switzerland (axelseguin95@gmail.com, daniel.kressner@epfl.ch)

Related work. In Euclidean space, the classical solution of the Hermite interpolation problem utilizes piecewise cubic polynomials [Far02]. This solution can be characterized in (at least) three different ways: (i) it minimizes the integral of the squared acceleration over the set of admissible interpolating curves, (ii) it is the unique piecewise cubic polynomial interpolating the points and the derivatives, (iii) it can be constructed with a geometric algorithm introduced by de Casteljau [dC59] involving iterated linear interpolation between suitably chosen control points. As we explain in the following, each of these characterizations can be generalized to manifolds. However, unlike for the Euclidean case, each characterization and extension produces a different curve.

(i) Extending the variational characterization is straightforward: the second derivative (acceleration) is replaced by the covariant derivative of the velocity vector and the search space is constrained to curves on the manifold [CSLC95] [ZN19] that satisfy the interpolation constraints. The solution to this variational problem, also known as Riemannian cubic, can be computed by numerical methods for boundary value differential problems, such as shooting methods [BCC21].

(ii) Exploiting the polynomial characterization of the solution requires one to recast manifold interpolation into an Euclidean setting. Several strategies have been explored for this purpose, e.g., a local linearization can be obtained from a (local) bijection between the manifold and a tangent space. For Hermite interpolation, Zimmermann [Zim20] proposes to use the Riemannian logarithmic map and its differential to map points and derivatives to the tangent space at one of the data points. Standard techniques, including polynomial interpolation, can then be used to construct the interpolation curve on the tangent space and map it back to the manifold with the Riemannian exponential map. We refer to [ZB22] for a recent extension to the multivariate setting.

(iii) The geometric nature of the de Casteljau algorithm lends itself to an intrinsic definition on manifolds. In fact, transplanting into a manifold setting simply requires to replace the linear segments that define the algorithm with geodesic segments, noting that geodesics are the manifold generalization of straight lines. This idea was pioneered by Park and Ravani in [PR95]; it has been adapted to solve the Hermite interpolation problem on spheres and compact Lie groups by Crouch and Leite [CKSL99] and on general Riemannian manifolds by Popiel and Noakes [PN07]. Rodriguez et al. [RSLJ05] proposed a similar approach, where the classical de Casteljau algorithm is interpreted and generalized as the weighted average of two curve branches satisfying the interpolating conditions. This blending technique is adapted to the manifold setting using geodesic branches and geodesic averaging, which – at least in principle – allows one to perform Hermite interpolation on a large class of manifolds even if the work [RSLJ05] itself focuses on compact Lie groups and the sphere.

The non-exhaustive list of algorithms above aims at illustrating that most approaches proposed so far focus on relatively simple manifolds: compact Lie groups, symmetric spaces like the sphere or complete Riemannian manifolds. Most of these techniques require to have closed-form expressions or at least a numerically tractable method for computing endpoint geodesics or the Riemannian exponential and logarithmic maps. For instance, for the case of the Stiefel manifold, the exponential map under the canonical metric has a closed-form expression [EAS99, §2.4.2] and an algorithm to approximate the corresponding logarithmic map has been proposed in [Zim17]. In contrast, for the manifold of fixed-rank matrices we are not aware of a computationally efficient way to realize the logarithmic map; a closed-form expression for the exponential map (under a suitable quotient geometry) is given in [AAM14, §6].

A first step towards relaxing computational requirements has been put forth by Polthier and Nava-Yazdani [NYP13] by generalizing the de Casteljau algorithm to work with generic endpoint

curves instead of geodesics as building blocks. This enlarges the applicability of the algorithm to, e.g., polygonal surfaces. On the other hand, velocity constraints cannot be taken into account and the concatenation of two such generalized de Casteljau curves may result in a non-differentiable junction. These drawbacks of [NYP13] were addressed by Krakowski et al. [KMSLB17] for the case of the Stiefel manifold with a generalized de Casteljau algorithm that uses a novel class of endpoint curves, termed quasi-geodesics. This technique allows one to interpolate points on the Stiefel manifold with a globally C^1 curve but the velocity can only be prescribed at the starting point.

Contribution. In this work, we propose and analyze a new Hermite interpolation technique on Riemannian manifolds. Extending upon [KMSLB17, NYP13] in being able to handle velocity constraints, our approach utilizes retractions to construct a novel class of endpoint curves. Retractions can be thought as first-order approximations of the exponential map that are widely used in Riemannian optimization [AMS08, Bou23]. For a large class of manifolds and retractions, the inverse retraction is available in closed-form. Whenever this is the case, our method makes it possible to solve the Hermite interpolation problem in a numerically efficient way on a larger class of manifolds than those available until now.

Outline. In Section 2, we develop a retraction-based Hermite (RH) interpolation scheme on manifolds. The well-posedness of the method is guaranteed on retraction-convex sets, a generalization of geodesically convex sets that we define and develop in Section 3. A convergence analysis of the RH scheme is carried out in Section 4, extending well-known results on the convergence of Hermite interpolation on Euclidean space for sufficiently smooth data. Finally, in Section 5, we demonstrate several applications of our novel interpolation scheme for both the manifold of fixed-rank matrices and the Stiefel manifold.

Mathematical setting. We recall some basic definitions of Riemannian geometry needed throughout this paper; see [Lee18] for details. Let \mathcal{M} denote a D -dimensional connected manifold endowed with a Riemannian metric g and the corresponding Levi-Civita connection ∇ . The tangent space at $x \in \mathcal{M}$ is denoted by $T_x\mathcal{M}$ and $T\mathcal{M} := \{(x, v) : x \in \mathcal{M}, v \in T_x\mathcal{M}\}$ denotes the tangent bundle. When \mathcal{M} is an embedded Riemannian submanifold, we let $N_x\mathcal{M}$ denote the normal space at $x \in \mathcal{M}$ and Π_x the orthogonal projection onto the tangent space at x . The Riemannian metric defines an inner product $\langle \cdot, \cdot \rangle_x$ on each tangent space $T_x\mathcal{M}$, with the induced norm $\|\cdot\|_x$. We let $d : \mathcal{M} \times \mathcal{M} \rightarrow [0, +\infty)$ denote the Riemannian distance function defined for any $x, y \in \mathcal{M}$ by

$$d(x, y) := \inf_{\delta \in \Gamma_{x,y}} L(\delta), \quad (1)$$

where $\Gamma_{x,y}$ contains every piecewise differentiable curve $\delta : [0, 1] \rightarrow \mathcal{M}$ joining x and y , and $L(\delta) := \int_0^1 \|\dot{\delta}(\tau)\|_{\delta(\tau)} d\tau$ denotes its length. This also allows us to define the open ball centered in x of radius r as

$$B(x, r) := \{y \in \mathcal{M} : d(x, y) < r\}. \quad (2)$$

For $x \in \mathcal{M}$, the Riemannian exponential $\text{Exp}_x : T_x\mathcal{M} \rightarrow \mathcal{M}$ maps a tangent vector $v \in T_x\mathcal{M}$ to $\gamma_{x,v}(1)$, where $\gamma_{x,v} : [0, 1] \rightarrow \mathcal{M}$ denotes the unique geodesic such that $\gamma_{x,v}(0) = x$ and $\dot{\gamma}_{x,v}(0) = v$. In general, such a geodesic is well-defined (and smooth) only for v in a neighborhood of $0 \in T_x\mathcal{M}$ and

locally invertible. The Riemannian logarithm Log_x is defined as the local inverse of the Riemannian exponential.

The mathematical formulation of the manifold Hermite interpolation problem is the following.

Problem 1. Given $N + 1$ tangent bundle data points $\{(p_i, v_i)\}_{i=0}^N \in T\mathcal{M}$ and scalar parameters $t_0 < t_1 < \dots < t_N$, find a continuously differentiable curve $H : [t_0, t_N] \rightarrow \mathcal{M}$ such that

$$\begin{cases} H(t_i) = p_i, \\ \dot{H}(t_i) = v_i, \end{cases} \quad \forall i = 0, \dots, N.$$

2 Generalized de Casteljau algorithm with retractions

The classical de Casteljau algorithm [dC59] is a geometric procedure to construct polynomial curves in \mathbb{R}^D . To describe the algorithm, let $\sigma_1(t; x, y) := (1 - t)x + ty$ denote the linear interpolation between two points $x, y \in \mathbb{R}^D$. Given $N + 1$ so called *control points* $b_0, \dots, b_N \in \mathbb{R}^D$, the relation

$$\sigma_k(t; b_i, \dots, b_{i+k}) := \sigma_1(t; \sigma_{k-1}(t; b_i, \dots, b_{i+k-1}), \sigma_{k-1}(t; b_{i+1}, \dots, b_{i+k})), \quad i = 0, \dots, N - k,$$

is applied recursively for $k = N, N - 1, \dots, 2$ to define a polynomial curve σ_N of degree N such that

$$\begin{aligned} \sigma_N(0; b_0, \dots, b_N) &= b_0, \\ \sigma_N(1; b_0, \dots, b_N) &= b_N, \\ \dot{\sigma}_N(0; b_0, \dots, b_N) &= N\dot{\sigma}_1(0; b_0, b_1) = N(b_1 - b_0), \\ \dot{\sigma}_N(1; b_0, \dots, b_N) &= N\dot{\sigma}_1(1; b_{N-1}, b_N) = N(b_N - b_{N-1}), \end{aligned}$$

where $\dot{\sigma}_N$ denotes the derivative of σ_N with respect to t . Only the first and last control points are interpolated while the other points influence the shape of the curve. In [PR95] an extension to control points on a manifold \mathcal{M} was proposed that replaces σ_1 by the endpoint geodesic joining x and y . The same recursive relation then yields a manifold curve verifying analogous properties: (a) it is smooth, (b) it interpolates the first and last points, and (c) the derivatives at the first and last points only depend on the first and last two control points, respectively. Property (c) allows one to conveniently control the endpoint derivatives via the choice of b_1, b_{N-1} , a property that makes the de Casteljau algorithm useful for Hermite interpolation; see, e.g., [PN07].

Along the line of work by Krakowski et al. [KMSLB17], we consider a generalization of the de Casteljau algorithm that allows for arbitrary smooth manifold curves at each step of the recursion (instead of constructing everything on top of geodesics). If each curve chosen to define the algorithm joins the prescribed endpoints then properties (a) and (b) are trivially satisfied. In [KMSLB17, Proposition 13], sufficient conditions for the chosen curves to produce property (c) are given for $N = 2$. The following proposition extends these results to $N = 3$.

Proposition 1. For $b_0, b_1, b_2, b_3 \in \mathcal{M}$ consider, as in Figure 1:

- smooth $\beta_i : [0, 1] \rightarrow \mathcal{M}$ joining b_i and b_{i+1} for each $i = 0, 1, 2$,
- smooth $\beta_{01} : [0, 1]^2 \rightarrow \mathcal{M}$ such that $\beta_{01}(\cdot, t)$ joins $\beta_0(t)$ and $\beta_1(t)$ for every $t \in [0, 1]$,

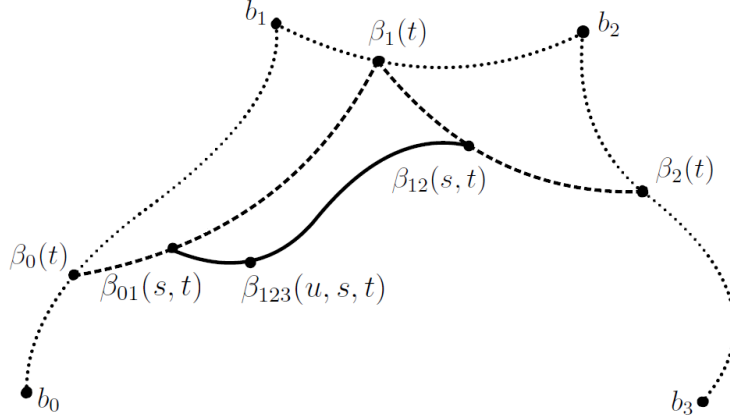


Figure 1: Generalized de Casteljau with 4 control points.

- smooth $\beta_{12} : [0, 1]^2 \rightarrow \mathcal{M}$ such that $\beta_{12}(\cdot, t)$ joins $\beta_1(t)$ and $\beta_2(t)$ for every $t \in [0, 1]$,
- smooth $\beta_{012} : [0, 1]^3 \rightarrow \mathcal{M}$ such that $\beta_{123}(\cdot, s, t)$ joins $\beta_{01}(s, t)$ and $\beta_{12}(s, t)$ for every $s, t \in [0, 1]$.

If, additionally,

- (i) $\beta_{01}(s, 0) = \beta_0(s)$ and $\beta_{12}(s, 1) = \beta_2(s)$,
- (ii) $\beta_{012}(s, 0, 0) = \beta_0(s)$ and $\beta_{012}(s, 1, 1) = \beta_2(s)$,

then the generalized de Casteljau manifold curve

$$\beta(t) = \beta_{012}(t, t, t)$$

satisfies

$$\beta(0) = b_0, \quad \beta(1) = b_3, \tag{3}$$

and

$$\dot{\beta}(0) = 3\dot{\beta}_0(0), \quad \dot{\beta}(1) = 3\dot{\beta}_2(1). \tag{4}$$

Proof. The interpolation condition (3) follows directly from the definitions:

$$\beta(0) = \beta_{012}(0, 0, 0) = \beta_{01}(0, 0) = \beta_0(0) = b_0$$

and, analogously, $\beta(1) = b_3$. To prove (4), we first note that

$$\dot{\beta}(t) = \frac{d}{ds}\beta_{012}(s, t, t)|_{s=t} + \frac{d}{ds}\beta_{012}(t, s, t)|_{s=t} + \frac{d}{ds}\beta_{012}(t, t, s)|_{s=t}.$$

At $t = 0$, inserting the definitions of the curves as well as conditions (i) and (ii) we thus obtain

$$\begin{aligned} \dot{\beta}(0) &= \frac{d}{ds}\beta_{012}(s, 0, 0)|_{s=0} + \frac{d}{ds}\beta_{012}(0, s, 0)|_{s=0} + \frac{d}{ds}\beta_{012}(0, 0, s)|_{s=0} \\ &= \dot{\beta}_0(0) + \frac{d}{ds}\beta_{01}(s, 0)|_{s=0} + \frac{d}{ds}\beta_{01}(0, s)|_{s=0} = 3\dot{\beta}_0(0). \end{aligned}$$

Analogously, one establishes $\dot{\beta}(1) = 3\dot{\beta}_2(1)$, which completes the proof. □ □

When one employs the same type of endpoint curve to define each $\beta_0, \dots, \beta_{012}$ in Proposition 1, such as endpoint geodesics or endpoint quasi-geodesics as proposed by [KMSLB17], then conditions (i) and (ii) are trivially satisfied. With this simplification, a result of the form (4) for a generalized de Casteljau algorithm of arbitrary order N can be found in [NYP13, Theorem 8]. However, to be useful for Hermite interpolation, we need to have explicit relationships between the control points and $\dot{\beta}_0(0)$ as well as $\dot{\beta}_2(1)$. While both are available for geodesics, only the first relationship can be made explicit for quasi-geodesics. Consequently, the interpolation problem considered in [KMSLB17] incorporates a velocity constraint at the first interpolation point only. In the next section we propose a new family of endpoint curves for defining curves $\beta_0, \dots, \beta_{012}$ that satisfy Proposition 1 and yield explicit relationships between the control points and $\beta_0(0), \beta_2(1)$.

2.1 A family of endpoint retraction curves

We use retractions [Bou23, Definition 3.47] to construct endpoint manifold curves. A retraction R is a smooth map from the tangent bundle $T\mathcal{M}$ to the manifold defined in a neighborhood of the origin of each tangent space. Letting R_x denote the restriction of R onto $T_x\mathcal{M}$ (that is, $R_x(v) = R(x, v)$), one additionally requires that $R_x(0) = x$ and $DR_x(0) = I_{T_x\mathcal{M}}$, the identity map of the tangent space.

The latter condition, also known as local rigidity, guarantees that any retraction is locally invertible; we denote the inverse retraction as R_x^{-1} .

Definition 2. *Given $x, y \in \mathcal{M}$ and $r \in [0, 1]$, the r -endpoint retraction curve joining x and y is defined as*

$$c_r(t; x, y) = R_{q(r)} \left((1-t)R_{q(r)}^{-1}(x) + tR_{q(r)}^{-1}(y) \right)$$

where $q(r) = R_x(rR_x^{-1}(y))$.

The choice of $r \in [0, 1]$ determines the anchor point for the retraction curve that defines c_r . Here and in the following two sections, we assume that any use of the retraction and its inverse is well-defined. For example, this is the case for Definition 2 for any $r \in [0, 1]$ when x and y are sufficiently close. A more precise statement on the well-posedness of r -endpoint retraction curves can be found in Proposition 10 below.

Proposition 3. *The r -endpoint retraction curve family satisfies the following properties:*

- (i) $c_r(0; x, y) = x$ and $c_r(1; x, y) = y$ for every $r \in [0, 1]$;
- (ii) $\dot{c}_0(0; x, y) = R_x^{-1}(y)$ and $\dot{c}_1(1; x, y) = -R_y^{-1}(x)$.

Proof. The definition of c_r directly implies (i). To show (ii), we first note that

$$\dot{c}_r(t; x, y) = DR_{q(r)} \left((1-t)R_{q(r)}^{-1}(x) + tR_{q(r)}^{-1}(y) \right) \left[R_{q(r)}^{-1}(y) - R_{q(r)}^{-1}(x) \right].$$

Because $q(0) = x$ and $q(1) = y$, the local rigidity of the retraction yields

$$\begin{aligned} \dot{c}_0(0; x, y) &= DR_x(0) [R_x^{-1}(y)] = R_x^{-1}(y), \\ \dot{c}_1(1; x, y) &= DR_y(0) [-R_y^{-1}(x)] = -R_y^{-1}(x). \end{aligned}$$

□

□

Note that c_r is not invariant under exchanging the endpoints, that is $c_r(t; x, y)$ does not coincide with $c_r(1-t; y, x)$ in general, unless the exponential map itself is chosen as retraction. On the other hand, extreme members of the family are related via $c_0(t; x, y) = c_1(1-t; y, x)$.

We will now explain how c_r is used to define curves that satisfy the conditions of Proposition 1 and, in turn, to define a suitable generalization of the de Casteljau algorithm. From Proposition 3 (ii) and (4), it follows that $\beta_0(\cdot) = c_0(\cdot; b_0, b_1)$ and $\beta_2(\cdot) = c_1(\cdot; b_2, b_3)$ are canonical choices for joining b_0 with b_1 and b_2 with b_3 , respectively. The other curves must be suitably chosen from the r -endpoint retraction curve family in order to satisfy Proposition 1.

Proposition 4. *The following choices of β_0 , β_1 , β_2 , β_{01} , β_{12} and β_{012} satisfy the conditions of Proposition 1:*

- $\beta_0(t) = c_0(t; b_0, b_1)$, $\beta_1(t) = c_{r_1(t)}(t; b_1, b_2)$, $\beta_2(t) = c_1(t; b_2, b_3)$,
- $\beta_{01}(s, t) = c_{r_{01}(s, t)}(s; \beta_0(t), \beta_1(t))$, $\beta_{12}(s, t) = c_{r_{12}(s, t)}(s; \beta_1(t), \beta_2(t))$,
- $\beta_{012}(u, s, t) = c_{r_{012}(u, s, t)}(u; \beta_{01}(s, t), \beta_{12}(s, t))$,

for any smooth functions $r_1 : [0, 1] \rightarrow [0, 1]$, $r_{01}, r_{12} : [0, 1]^2 \rightarrow [0, 1]$ and $r_{012} : [0, 1]^3 \rightarrow [0, 1]$ such that

$$r_{01}(s, 0) = 0, \quad r_{12}(s, 1) = 1, \quad r_{012}(s, 0, 0) = 0, \quad r_{012}(s, 1, 1) = 1.$$

Moreover, the resulting manifold curve $\beta(t) = \beta_{012}(t, t, t)$ satisfies

$$\dot{\beta}(0) = 3\dot{c}_0(0; b_0, b_1) = 3R_{b_0}^{-1}(b_1), \quad \dot{\beta}(1) = 3\dot{c}_1(1; b_2, b_3) = -3R_{b_3}^{-1}(b_2). \quad (5)$$

Proof. Proposition 3 (i) implies that the curves β_0 , β_1 , β_2 , $\beta_{01}(\cdot, t)$, $\beta_{12}(\cdot, t)$ and $\beta_{012}(\cdot, s, t)$ have the correct endpoints for every $s, t \in [0, 1]$ and any choice of r_1 , r_{01} , r_{12} and r_{012} . Direct computation shows the remaining requirements (i) and (ii) of Proposition 1:

- (i) $\beta_{01}(s, 0) = c_{r_{01}(s, 0)}(s; \beta_0(0), \beta_1(0)) = c_0(s; b_0, b_1) = \beta_0(s)$,
 $\beta_{12}(s, 1) = c_{r_{12}(s, 1)}(s; \beta_1(1), \beta_2(1)) = c_1(s; b_2, b_3) = \beta_2(s)$,
- (ii) $\beta_{012}(s, 0, 0) = c_{r_{012}(s, 0, 0)}(s; \beta_{01}(0, 0), \beta_{12}(0, 0)) = c_0(s; b_0, b_1) = \beta_0(s)$,
 $\beta_{012}(s, 1, 1) = c_{r_{012}(s, 1, 1)}(s; \beta_{01}(1, 1), \beta_{12}(1, 1)) = c_1(s; b_2, b_3) = \beta_2(s)$.

Finally, the relation (5) follows from combining (4) with Proposition 3 (ii). □ □

Proposition 4 offers a great degree of flexibility in choosing r_1 , r_{01} , r_{12} , and r_{012} . For practical purposes, a simple choice that leads to a computationally inexpensive evaluation of the curve is preferable. We propose to choose

$$r_1(s) = 1/2, \quad r_{01}(s, t) = 0, \quad r_{12}(s, t) = 1, \quad r_{012}(u, s, t) = t. \quad (6)$$

By choosing constant r_{01} and r_{12} , the evaluation of each of the intermediate curves β_{01} and β_{12} requires one retraction and one inverse retraction only for every value of (s, t) . For any other choice of r_{01} or r_{12} satisfying Proposition 4, these evaluations require two retractions and three inverse retractions. In total, as we will see below in Algorithm 2, the choice (6) essentially consists of 7 retractions and 5 inverse retractions per evaluation of the generalized de Casteljau manifold curve, ignoring the cost for preprocessing.

At this point, the choice of $r_1(s) = 1/2$ appears to be ad hoc, especially because Proposition 4 imposes no constraint on r_1 . As we will see in Section 5.2.5, this choice of r_1 is crucial for the scheme to attain favorable convergence properties. From now on, we restrict ourselves to (6).

Definition 5. Given control points $b_0, b_1, b_2, b_3 \in \mathcal{M}$ we use $\beta(\cdot; b_0, b_1, b_2, b_3)$ to denote the generalized de Casteljau curve constructed in Proposition 4 with the choice (6) for $r_1, r_{01}, r_{12}, r_{012}$.

2.2 The retraction-based Hermite (RH) interpolation scheme

The generalized de Casteljau curve of Definition 5 will now be used to solve the Hermite interpolation problem, Problem 1, by choosing suitable control points.

Proposition 6. Given $(p_0, v_0), (p_1, v_1) \in T\mathcal{M}$, define

$$p_0^+ = R_{p_0} \left(\frac{1}{3} v_0 \right), \quad p_1^- = R_{p_1} \left(-\frac{1}{3} v_1 \right)$$

and let $\alpha(t) \equiv \alpha(t; p_0, v_0, p_1, v_1) := \beta(t; p_0, p_0^+, p_1^-, p_1)$ denote the generalized de Casteljau curve according to Definition 5. Then

$$\alpha(0) = p_0, \quad \alpha(1) = p_1, \quad \dot{\alpha}(0) = v_0, \quad \dot{\alpha}(1) = v_1.$$

Proof. The result follows from combining Propositions 1 and 4:

$$\begin{aligned} \alpha(0) &= \beta(0; p_0, p_0^+, p_1^-, p_1) = p_0, \quad \alpha(1) = \beta(1; p_0, p_0^+, p_1^-, p_1) = p_1, \\ \dot{\alpha}(0) &= \dot{\beta}(0; p_0, p_0^+, p_1^-, p_1) = 3R_{p_0}^{-1}(p_0^+) = 3R_{p_0}^{-1} \left(R_{p_0} \left(\frac{1}{3} v_0 \right) \right) = v_0, \\ \dot{\alpha}(1) &= \dot{\beta}(1; p_0, p_0^+, p_1^-, p_1) = -3R_{p_1}^{-1}(p_1^-) = -3R_{p_1}^{-1} \left(R_{p_1} \left(-\frac{1}{3} v_1 \right) \right) = v_1. \end{aligned}$$

□

□

As an immediate consequence of Proposition 6, the following corollary shows how α is used piecewise to define the *retraction-based Hermite (RH) interpolant* H that addresses Problem 1.

Corollary 7. Letting $h_i := t_{i+1} - t_i$ for $i = 0, \dots, N-1$, the manifold curve $H : [t_0, t_N] \rightarrow \mathcal{M}$ defined piecewise by

$$H(t)|_{[t_i, t_{i+1}]} = \alpha \left(\frac{t - t_i}{h_i}; p_i, h_i v_i, p_{i+1}, h_i v_{i+1} \right), \quad i = 0, \dots, N-1, \quad (7)$$

is a solution to Problem 1.

Algorithms 1 and 2 summarize the construction of H and its evaluation, respectively. We separate the computations needed for evaluating the RH interpolant (online phase) from those that can be precomputed, stored and used in every evaluation (offline phase).

Algorithm 1 Offline Phase (precompute quantities defining the RH interpolant)

Input: Tangent bundle data points $\{(p_i, v_i)\}_{i=0}^N \in T\mathcal{M}$, $t_0 < t_1 < \dots < t_N$.

- 1: **for** $i = 0, \dots, N-1$ **do**
 - 2: $h_i = t_{i+1} - t_i$;
 - 3: $p_i^+ = R_{p_i}(\frac{1}{3}h_i v_i)$;
 - 4: $p_{i+1}^- = R_{p_{i+1}}(-\frac{1}{3}h_i v_{i+1})$;
 - 5: $q_i = R_{p_i^+}(\frac{1}{2}R_{p_i^+}^{-1}(p_{i+1}^-))$; ▷ Anchor for the middle segment β_1 .
 - 6: $w_i^+ = R_{q_i}^{-1}(p_i^+)$; ▷ Tangent vector from q_i to p_i^+
 - 7: $w_{i+1}^- = R_{q_i}^{-1}(p_{i+1}^-)$; ▷ Tangent vector from q_i to p_{i+1}^-
 - 8: **end for**
 - 9: **return** : $\{q_i, w_i^+, w_{i+1}^-\}_{i=0}^{N-1}$;
-

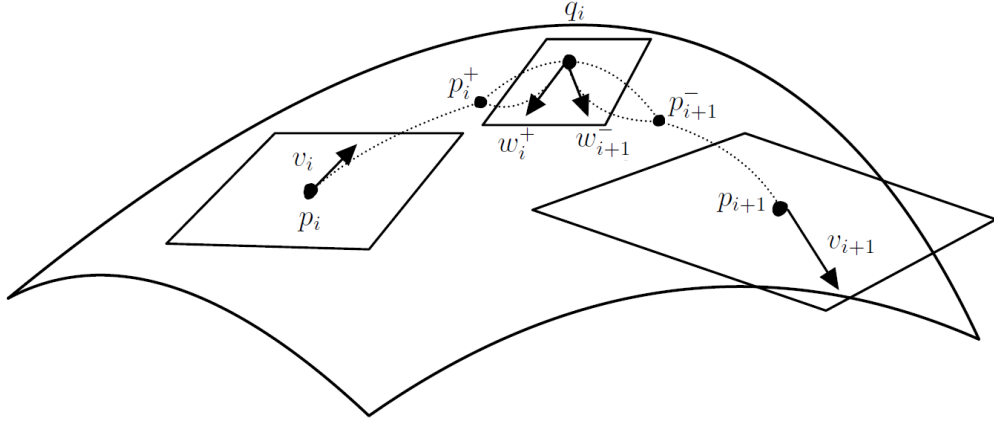


Figure 2: Illustration of offline computations performed by Algorithm 1. Parallelograms indicate tangent spaces whereas dotted lines indicate retraction curves.

3 Retraction-convex sets

The notion of an r -endpoint retraction curve c_r from Definition 2 is the central ingredient of our RH interpolation. To guarantee that the (inverse) retractions involved in c_r and, in turn, c_r itself are well-defined, we introduce the notion of a retraction-convex set.

The definition of retraction-convex set is made possible by the local rigidity property of retractions ensuring the existence of their local inverse. The following property [Bou23, Corollary 10.27] conveniently characterizes the subset of the retraction's domain over which the inverse retraction can be defined.

Proposition 8. *For any retraction R there exists a continuous function $\Delta : \mathcal{M} \rightarrow (0, \infty]$ defining a subset $\mathcal{T} := \{(x, v) \in T\mathcal{M} : \|v\|_x < \Delta(x)\}$ of the tangent bundle such that*

$$E : \mathcal{T} \subset T\mathcal{M} \rightarrow \mathcal{M} \times \mathcal{M}$$

$$(x, v) \mapsto (x, R_x(v))$$

is a diffeomorphism.

Algorithm 2 Online Phase (evaluation of RH interpolant at t)

Input: $t \in [t_0, t_N]$, $\{p_i, v_i, t_i\}_{i=0}^N$, $\{q_i, w_i^+, w_{i+1}^-\}_{i=0}^{N-1}$;

- 1: Find largest $i \in \{0, \dots, N-1\}$ such that $t_i \leq t$;
 - 2: $h_i = t_{i+1} - t_i$;
 - 3: $\tau = \frac{t-t_i}{h_i}$;
 - 4: $\beta_0 = R_{p_i} \left(\frac{\tau}{3} h_i v_i \right)$; $\triangleright 1 \times R$
 - 5: $\beta_1 = R_{q_i} \left((1-\tau) w_i^+ + \tau w_{i+1}^- \right)$; $\triangleright 1 \times R$
 - 6: $\beta_2 = R_{p_{i+1}} \left(-\frac{\tau}{3} h_i v_{i+1} \right)$; $\triangleright 1 \times R$
 - 7: $\beta_{01} = c_0(\tau; \beta_0, \beta_1)$; $\triangleright 1 \times R + 1 \times R^{-1}$
 - 8: $\beta_{12} = c_1(\tau; \beta_1, \beta_2)$; $\triangleright 1 \times R + 1 \times R^{-1}$
 - 9: **return** $\beta = c_\tau(\tau; \beta_{01}, \beta_{12})$; $\triangleright 2 \times R + 3 \times R^{-1}$
-

Accordingly, if $v \in T_x \mathcal{M}$ is such that $\|v\|_x < \Delta(x)$, then the retraction is well-defined. Likewise, whenever $x, y \in \mathcal{M}$ are such that $(x, y) \in E(\mathcal{T})$, we say that the inverse retraction $R_x^{-1}(y)$ is well-defined and is equal to the unique $v \in T_x \mathcal{M}$ such that $E(x, v) = (x, y)$. Moreover, with this definition the inverse retraction is smooth both in x and y .

Definition 9. A set $\mathcal{U} \subset \mathcal{M}$ is said to be retraction-convex if for any $x, y, z \in \mathcal{U}$

- (i) the inverse retraction $R_x^{-1}(y)$ is well-defined,
- (ii) $R_x((1-\tau)R_x^{-1}(y) + \tau R_x^{-1}(z))$ is well-defined for every $\tau \in [0, 1]$ and belongs to \mathcal{U} ,

An equivalent characterization of retraction-convexity is that the inverse retraction R_x^{-1} is well-defined on \mathcal{U} and the image of \mathcal{U} through the inverse retraction is a convex subset of $T_x \mathcal{M}$ for every $x \in \mathcal{U}$. Retraction-convex sets generalize geodesically convex sets [Lee18, §6]: instead of the geodesic it is the endpoint retraction curve between two points that remains in the set.

Proposition 10. Let \mathcal{U} be retraction-convex and $x, y \in \mathcal{U}$. Then the r -endpoint retraction curve $t \mapsto c_r(t; x, y)$ is well-defined for every $t, r \in [0, 1]$.

Proof. By Definition 9 (i), $R_x^{-1}(y)$ is well-defined. Now using Definition 9 (ii) with $z = x$ and $\tau = 1 - r$, we find that $q(r) = R_x(rR_x^{-1}(y))$ is well-defined and belongs to \mathcal{U} . Therefore, the inverse retractions $R_{q(r)}^{-1}(x)$ and $R_{q(r)}^{-1}(y)$ are also well-defined and the proof is completed by applying once again Definition 9 (ii). \square \square

Proposition 11. For a retraction-convex set \mathcal{U} consider control points $b_0, b_1, b_2, b_3 \in \mathcal{U}$. Then the generalized de Casteljau curve $t \mapsto \beta(t; b_0, b_1, b_2, b_3)$ constructed in Definition 5 is well defined for every $t \in [0, 1]$.

Proof. We apply recursively the result of Proposition 10. Since $b_0, b_1, b_2, b_3 \in \mathcal{U}$, the curves $\beta_0, \beta_1, \beta_2$ are well-defined and their image is entirely contained in \mathcal{U} . In turn, this implies that for every $t \in [0, 1]$ the curves $\beta_{01}(\cdot, t)$ and $\beta_{12}(\cdot, t)$ are well-defined and their image is entirely contained in \mathcal{U} . Finally, it follows that for every $s, t \in [0, 1]^2$ the curve $\beta_{012}(\cdot, s, t)$ is well-defined. \square \square

Note that this proof is valid for any generalized de Casteljau curve constructed as in Proposition 4.

3.1 Existence of retraction-convex sets

In the special case that the retraction is the exponential map, retraction-convexity coincides with geodesic convexity. The existence of geodesically convex neighborhoods around any manifold point is shown for instance by do Carmo [dC92, Proposition 4.2].¹ The proof is based on the Gauss lemma [dC92, Lemma 3.5], a result from Riemannian geometry that crucially relies on the exponential map which does not extend to general retraction curves. Instead, our proof will only use properties of the manifold distance function, sharing common features with the proof [dC92, Theorem 3.3.7] that shows the existence of totally retractive neighborhoods as defined in [HAG15, Section 3.3].

Theorem 12. *For every $x \in \mathcal{M}$ there exists $\bar{\rho} > 0$ such that for any $\rho < \bar{\rho}$, the manifold ball $B(x, \rho)$ defined in (2) is retraction-convex.*

Given a $\bar{\rho} > 0$ satisfying Theorem 12, then the property is also satisfied by $\eta\bar{\rho}$, for any $\eta \in (0, 1)$. Thus, to fix a single value for each $x \in \mathcal{M}$, we denote

$$\bar{\rho}(x) := \sup \{ \bar{\rho} > 0 : B(x, \rho) \text{ is retraction-convex } \forall \rho < \bar{\rho} \}. \quad (8)$$

The proof of Theorem 12 uses the following lemma.

Lemma 13. *For every $x \in \mathcal{M}$ and any $v \in T_x\mathcal{M}$ we have*

$$\frac{d^2}{dt^2} d(x, R_x(tv))^2 \Big|_{t=0} = 2 \|v\|_x^2.$$

Proof. Setting $c(t) := R_x(tv)$, it follows from [Lee18, Proposition 6.11] that

$$d(x, c(t))^2 = \|\text{Log}_x(c(t))\|_x^2$$

for sufficiently small $|t|$. This allows us to explicitly compute

$$\frac{d}{dt} d(x, c(t))^2 = 2 \langle \text{DLog}_x(c(t))[\dot{c}(t)], \text{Log}_x(c(t)) \rangle_x,$$

and

$$\begin{aligned} \frac{d^2}{dt^2} d(x, c(t))^2 &= 2 \langle \text{D}^2 \text{Log}_x(c(t))[\dot{c}(t), \dot{c}(t)] + \text{DLog}_x(c(t))[\ddot{c}(t)], \text{Log}_x(c(t)) \rangle_x \\ &\quad + 2 \|\text{DLog}_x(c(t))[\dot{c}(t)]\|_x^2. \end{aligned}$$

Using that $c(0) = x$, the first term vanishes at $t = 0$ because $\text{Log}_x(c(0)) = \text{Log}_x(x) = 0$. Using local rigidity, $\text{DLog}_x(x) = I_{T_x\mathcal{M}}$, and $\dot{c}(0) = v$ completes the proof: $\frac{d^2}{dt^2} d(x, c(t))^2 \Big|_{t=0} = 2 \|\text{DLog}_x(x)[v]\|_x^2 = 2 \|v\|_x^2$. \square \square

Proof. (of Theorem 12) Given $x \in \mathcal{M}$, consider the function $f : T\mathcal{M} \rightarrow \mathbb{R}$

$$f(y, v) = d(x, R_y(v))^2.$$

¹Note that [dC92] uses the term strongly convex set instead of geodesically convex set.

The squared Riemannian distance function is smooth on a neighborhood of the diagonal of $\mathcal{M} \times \mathcal{M}$ [Lee18, Lemma 6.8] and by definition the retraction R is smooth on its domain (a neighborhood of the zero section of $T\mathcal{M}$). Therefore the function f is smooth on an open neighborhood of $(x, 0)$ in $T\mathcal{M}$.

We will first establish a (local) convexity property of f . Using $\nabla_T^2 f(x, w)$ to denote the (Euclidean) Hessian of $f(x, \cdot)$ at $w \in T_x\mathcal{M}$, the result of Lemma 13 can be rephrased as

$$\langle \nabla_T^2 f(x, 0) [v], v \rangle_x = 2 \|v\|_x^2.$$

In particular, this shows that $\nabla_T^2 f(x, 0)$ is positive definite.

By smoothness, there exists a neighborhood $V \subset T\mathcal{M}$ containing $(x, 0)$ such that $\nabla_T^2 f(y, v)$ remains positive definite at every $(y, v) \in V$.

For an arbitrary subset $S \subseteq T\mathcal{M}$, we let

$$\begin{aligned} \pi_{\mathcal{M}}(S) &:= \{y \in \mathcal{M} : \exists v \in T_y\mathcal{M} \text{ such that } (y, v) \in S\}, \\ \pi_{T_y\mathcal{M}}(S) &:= \{v \in T_y\mathcal{M} : (y, v) \in S\}. \end{aligned}$$

For every $y \in \pi_{\mathcal{M}}(V)$ the function $f(y, \cdot)$ is convex on any convex subset of $\pi_{T_y\mathcal{M}}(V)$.

The set V is an open set in the atlas topology of $T\mathcal{M}$, associated with the natural smooth structure of $T\mathcal{M}$ [Lee03, Lemma 4.1]. This means that for any local chart (\mathcal{U}, ϕ) of \mathcal{M} , the set $\psi_\phi(\pi_{\mathcal{M}}^{-1}(\mathcal{U}) \cap V)$ is an open subset of \mathbb{R}^{2D} , where

$$\pi_{\mathcal{M}}^{-1}(\mathcal{U}) = \{(y, v) \in T\mathcal{M} : y \in \mathcal{U}, v \in T_y\mathcal{M}\}$$

and

$$\begin{aligned} \psi_\phi : \pi_{\mathcal{M}}^{-1}(\mathcal{U}) \cap V &\rightarrow \mathbb{R}^{2D} \\ (y, v) &\mapsto (\phi(y), \lambda) \end{aligned}$$

with $\lambda \in \mathbb{R}^D$ being the coordinates of v in the basis of $T_y\mathcal{M}$ formed by the partial derivatives of the inverse local charts, that is $v = \sum_{i=1}^D \lambda_i \partial_i \phi^{-1}(\phi(y))$.

Now consider a local chart such that $x \in \mathcal{U}$. Because $\psi_\phi(\pi_{\mathcal{M}}^{-1}(\mathcal{U}) \cap V)$ is an open subset of \mathbb{R}^{2D} that contains $(\phi(x), 0)$, there exist $\varepsilon_{\mathcal{M}} > 0$ and $\varepsilon_T > 0$ such that

$$B_D(\phi(x), \varepsilon_{\mathcal{M}}) \times B_D(0, \varepsilon_T) \subseteq \psi_\phi(\pi_{\mathcal{M}}^{-1}(\mathcal{U}) \cap V),$$

where $B_D(\cdot, \cdot)$ denotes an open ball (in the Euclidean norm) of \mathbb{R}^D . By continuity of ψ_ϕ , its preimage is an open subset of V that contains $(x, 0)$:

$$\begin{aligned} W &:= \psi_\phi^{-1}(B_D(\phi(x), \varepsilon_{\mathcal{M}}) \times B_D(0, \varepsilon_T)) \\ &= \left\{ (y, v) \in T\mathcal{M} : y \in \phi^{-1}(B_D(\phi(x), \varepsilon_{\mathcal{M}})), v = \sum_{i=1}^D \lambda_i \partial_i \phi^{-1}(\phi(y)), \|\lambda\|_2 < \varepsilon_T \right\}. \end{aligned}$$

From Proposition 8, we have that E is a diffeomorphism on $W \cap \mathcal{T}$ (which is open in $T\mathcal{M}$) and so the set $E(W \cap \mathcal{T})$ is an open neighborhood of (x, x) . Thus, the constant

$$\bar{\rho} := \sup \{ \rho \geq 0 : B(x, \rho) \times B(x, \rho) \subseteq E(W \cap \mathcal{T}) \}.$$

is strictly positive.

The statement of the theorem is proven by showing that the set $B(x, \rho)$ is retraction-convex for any $\rho < \bar{\rho}$. Definition 9 (i) follows from the invertibility of E on $B(x, \rho) \times B(x, \rho)$: For any $y, z \in B(x, \rho)$ there exists a unique $v \in T_y \mathcal{M}$ such that $E(y, v) = (y, z)$ and, hence, $v = R_y^{-1}(z)$ is well-defined. To establish Definition 9 (ii), consider arbitrary $w, y, z \in B(x, \rho)$. We first note that the set

$$\pi_{T_y \mathcal{M}}(W \cap \mathcal{T}) = \left\{ v \in T_y \mathcal{M} : v = \sum_{i=1}^D \lambda_i \partial_i \phi^{-1}(\phi(y)), \|\lambda\|_2 < \varepsilon_T, \|v\|_y < \Delta(y) \right\}$$

is convex (as the intersection of two convex sets) and in the domain of R_y . Both $R_y^{-1}(w)$ and $R_y^{-1}(z)$ are contained in $\pi_{T_y \mathcal{M}}(W \cap \mathcal{T})$ and hence the same holds for their convex linear combination. The convexity of $f(y, \cdot)$ on $\pi_{T_y \mathcal{M}}(W \cap \mathcal{T})$, a convex subset of $\pi_{T_y \mathcal{M}}(V)$, implies for every $t \in [0, 1]$ that

$$\begin{aligned} d(x, R_y((1-t)R_y^{-1}(w) + tR_y^{-1}(z)))^2 &= f(y, (1-t)R_y^{-1}(w) + tR_y^{-1}(z)) \\ &\leq (1-t)f(y, R_y^{-1}(w)) + tf(y, R_y^{-1}(z)) \\ &= (1-t)d(x, w)^2 + td(x, z)^2 < \rho^2, \end{aligned}$$

which proves the retraction-convexity of $B(x, \rho)$. □ □

4 Analysis of RH interpolation

For the purpose of deriving qualitative and asymptotic properties of RH interpolation, we suppose that the interpolation data are samples of a continuously differentiable manifold curve $\gamma : [0, 1] \rightarrow \mathcal{M}$, that is

$$p_i = \gamma(t_i), \quad v_i = \dot{\gamma}(t_i), \quad \forall i = 0, \dots, N, \quad (9)$$

for some $0 = t_0 < t_1 < \dots < t_N = 1$. Because of its piecewise definition (see Corollary 7), it is sufficient to consider the RH interpolant on a single subinterval, i.e. the manifold curve $H_h : [t, t+h] \rightarrow \mathcal{M}$ defined by

$$H_h(\tau) = \alpha \left(\frac{\tau - t}{h}; \gamma(t), h\dot{\gamma}(t), \gamma(t+h), h\dot{\gamma}(t+h) \right) \quad (10)$$

for sufficiently small $h > 0$ and $t \in [0, 1-h]$, satisfying $H_h(t) = \gamma(t)$, $H_h(t+h) = \gamma(t+h)$, $\dot{H}_h(t) = \dot{\gamma}(t)$, and $\dot{H}_h(t+h) = \dot{\gamma}(t+h)$. Our results for a single interval apply to the piecewise solution of (9) by letting $h = \max_{i=0, \dots, N-1} t_{i+1} - t_i$.

4.1 Lipschitz continuity of the retraction

Lemma 14 below states the Lipschitz continuity of (inverse) retractions. A very similar statement can be found in [RW12, Lemma 6], under a local equicontinuity assumption of the retraction derivatives. Our proof, reported in Appendix A together with the proof of Corollary 15, leverages Proposition 8 to avoid this assumption.

Lemma 14. For every $x \in \mathcal{M}$, there exist $L_R(x) > 0$ and $M_R(x) > 0$ such that

(i) for any $u, v \in \{w \in T_x \mathcal{M} : \|w\|_x < \Delta(x)/3\}$ we have

$$d(R_x(u), R_x(v)) \leq L_R(x) \|u - v\|_x, \quad (11)$$

(ii) for any $y, z \in \{R_x(w) \in \mathcal{M} : \|w\|_x < \Delta(x)/3\}$ we have

$$\|R_x^{-1}(y) - R_x^{-1}(z)\|_x \leq M_R(x) d(y, z), \quad (12)$$

with $\Delta(x) > 0$ defined in Proposition 8.

Corollary 15. For every compact set $K \subset \mathcal{M}$, inequalities (11) and (12) hold for every $x \in K$ with finite strictly positive constants $L_R(K)$ and $M_R(K)$ depending only on K .

Proof. This is a consequence of the more general Proposition 22, see Appendix A. □ □

4.2 Well-posedness of RH interpolation

Throughout the two upcoming sections we make the assumption that the function $x \in \mathcal{M} \rightarrow \bar{\rho}(x)$ defined by (8) is lower-bounded on the image of the curve γ by a strictly positive constant that we denote

$$\rho_{\min} := \inf_{\tau \in [0,1]} \bar{\rho}(\gamma(\tau)) > 0. \quad (13)$$

Since retractions are smooth, intuition suggests that the function $\bar{\rho}$ should be continuous, thereby guaranteeing the validity of this technical assumption.

By Proposition 11, the RH interpolation scheme is well-defined provided that the control points belong to a retraction-convex set. The following result is established that this indeed the case for sufficiently small h .

Proposition 16. There exists a constant $h_1 > 0$ depending on the curve γ and on the retraction such that for any $0 < h < h_1$ the RH interpolant H_h defined in (10) is well-posed for every $t \in [0, 1 - h]$.

Proof. By Proposition 6 and Corollary 7,

$$H_h(\tau) = \beta \left(\frac{\tau - t}{h}; p_0(t), p_0^+(t, h), p_1^-(t, h), p_1(t, h) \right),$$

with the control points

$$\begin{aligned} p_0(t) &:= \gamma(t), & p_1(t, h) &:= \gamma(t + h), \\ p_0^+(t, h) &:= R_{\gamma(t)}(h\dot{\gamma}(t)/3), & p_1^-(t, h) &:= R_{\gamma(t+h)}(-h\dot{\gamma}(t+h)/3). \end{aligned}$$

Denoting by L_γ a Lipschitz constant of the curve γ on $[0, 1]$ we have

$$d(p_0(t), p_1(t, h)) = d(\gamma(t), \gamma(t + h)) \leq L_\gamma h,$$

The function $\Delta(\cdot)$ defined in Proposition 8, is continuous and strictly positive so the quantity $\Delta_{\min} = \min_{\tau \in [0,1]} \Delta(\gamma(\tau))$ is strictly positive. If $h < \frac{\Delta_{\min}}{L_\gamma}$, then

$$\|h\dot{\gamma}(t)/3\|_{\gamma(t)} < \Delta(\gamma(t))/3, \quad \|h\dot{\gamma}(t+h)/3\|_{\gamma(t+h)} < \Delta(\gamma(t+h))/3.$$

This allows us to invoke Lemma 14-(i) with the constant $L_R(\gamma) := \sup_{t \in [0,1]} \{L_R(\gamma(t))\}$. This constant is finite by Corollary 15. We have

$$\begin{aligned} d(p_0(t), p_0^+(t, h)) &\leq hL_R \|\dot{\gamma}(t)/3\|_{\gamma(t)} \leq hL_R L_\gamma / 3, \\ d(p_0(t), p_1^-(t, h)) &\leq d(p_0(t), p_1(t, h)) + d(p_1(t, h), p_1^-(t, h)) \\ &\leq L_\gamma h + hL_R \|\dot{\gamma}(t+h)/3\|_{\gamma(t+h)} \leq L_\gamma(1 + L_R/3)h. \end{aligned}$$

Hence, if $h < \frac{\Delta_{\min}}{L_\gamma}$, then all control point of H_h are contained in $B(\gamma(t), Qh)$ with

$$Q := \max \{L_\gamma, L_R L_\gamma / 3, L_\gamma(1 + L_R/3)\} = L_\gamma(1 + L_R/3).$$

Therefore by taking $h < h_1 := \min \left\{ \frac{\Delta_{\min}}{L_\gamma}, \frac{\rho_{\min}}{Q} \right\}$ all the control points of H_h are contained in the retraction-convex set $B(\gamma(t), \rho_{\min})$. This implies the curve H_h is well-defined. \square \square

4.3 Interpolation error

In the Euclidean setting, asymptotic convergence rates of the maximum interpolation error are classic results of numerical analysis. For the case of piecewise cubic Hermite interpolation the error can be shown to converge as $O(h^4)$ [QSS07, Section 8.4], where h is the largest sampling step size. In this section, we generalize this result to the RH interpolation scheme.

Theorem 17. *Let $\gamma \in C^4([0, 1])$ and consider H_h , the RH interpolant of γ on a subinterval $[t, t+h]$ as defined in (10). Assume that γ satisfies (13) and that for $k = 2, 3, 4$ there exist constants $L_{RH}^{(k)} > 0$ and $h_2 > 0$ such that for every $0 < h < h_2$ and any $t \in [0, 1-h]$ it holds that*

$$\sup_{\tau \in [t, t+h]} \left\| \frac{D^k H_h(\tau)}{d\tau^k} \right\|_{H_h(\tau)} < L_{RH}^{(k)}, \quad (14)$$

where $\frac{D^k}{d\tau^k}$ denotes the order- k covariant derivative along a curve [Bou23, Sec. 10.7]. Then, there exist constants $\kappa > 0$ and $\bar{h} > 0$ depending on the curve γ , the manifold and the retraction such that for any $0 < h < \bar{h}$ and any $t \in [0, 1-h]$, we have

$$\max_{\tau \in [t, t+h]} d(\gamma(\tau), H_h(\tau)) < \kappa h^4.$$

The above result is independent of $t \in [0, 1-h]$, hence we can bound the maximum interpolation error of the full piecewise RH interpolant of the curve γ on the interval $[0, 1]$.

Corollary 18. *Under the assumptions of Theorem 17, the piecewise RH interpolant H of γ defined by (7) with data (9) verifies*

$$\max_{\tau \in [0,1]} d(\gamma(\tau), H(\tau)) < \kappa h^4,$$

where $h = \max_{i=0, \dots, N-1} t_{i+1} - t_i$.

The proof of Theorem 17 relies on a local linearization of the manifold: the interpolation curve H_h and the curve γ are represented in normal coordinates [Lee18, p. 132] around a point of the curve γ by applying the local inverse of the Riemannian exponential map. This is possible provided that the image of γ , the control points, and intermediate quantities involved in the procedure remain confined to a domain of invertibility of the exponential map as $h \rightarrow 0$. The following Lemmas 19 and 20 show that these requirements are met when considering sufficiently small h , reflecting the asymptotic nature of Theorem 17. In practice, our experiments suggest that the convergence order 4 established by the theorem can be observed as soon as the interpolation curve is well-defined; see the numerical experiments Section 5. This assumes that the scheme verifies assumption (14); see Section 5.2.5 for the importance of this assumption.

Lemma 19. *There exist a constants $L_{RH} > 0$ and $h_3 > 0$ depending on γ and on the retraction such that for every $0 < h < h_3$ and any $t \in [0, 1 - h]$*

$$d(H_h(\tau_1), H_h(\tau_2)) \leq L_{RH} |\tau_1 - \tau_2|, \quad \forall \tau_1, \tau_2 \in [t, t + h].$$

A proof of Lemma 19 can be found in Appendix B.2. Lipschitz continuity of H_h and of γ provides sufficient conditions to be able to represent the images of H_h and γ on the interval $[t, t + h]$ in normal coordinates around any point $\gamma(s)$, $s \in [t, t + h]$.

Lemma 20. *Denote $r_{\min} := \min_{\tau \in [0, 1]} \text{inj}(\gamma(\tau))$, the minimum of the injectivity radius of the Riemannian exponential map along the curve. There exists $h_4 > 0$ such that for every $0 < h < h_4$ and any $t \in [0, 1 - h]$ we have*

$$\begin{aligned} d(\gamma(s), \gamma(\tau)) &< r_{\min}, \\ d(\gamma(s), H_h(\tau)) &< r_{\min}, \end{aligned} \quad \forall s, \tau \in [t, t + h].$$

Proof. The constant r_{\min} is strictly positive by the continuity of the injectivity radius function [Bou23, Proposition 10.24] and compactness of the image of the curve. We take any $0 < h < h_4 := \min \left\{ \frac{r_{\min}}{2L_\gamma}, h_3, \frac{r_{\min}}{2L_{RH}} \right\}$ and consider an arbitrary $t \in [0, 1 - h]$. First of all, for any $s, \tau \in [t, t + h]$ we have

$$d(\gamma(s), \gamma(\tau)) \leq L_\gamma h < \frac{r_{\min}}{2} < r_{\min},$$

Furthermore, the requirement $h < h_3$ guarantees that H_h is well-defined and, by Lemma 19, that H_h is L_{RH} -Lipschitz continuous. Thus

$$\begin{aligned} d(\gamma(s), H_h(\tau)) &\leq d(\gamma(s), \gamma(t)) + d(\gamma(t), H_h(\tau)) < \frac{r_{\min}}{2} + d(H_h(t), H_h(\tau)) \\ &< \frac{r_{\min}}{2} + L_{RH} h \\ &< \frac{r_{\min}}{2} + \frac{r_{\min}}{2} = r_{\min}. \end{aligned}$$

□

□

Proof. (of Theorem 17) Take any $0 < h < h_4$, $t \in [0, 1 - h]$ and $s \in [t, t + h]$. By Lemma 20, we can express γ and H_h in normal coordinates. Define

$$\begin{aligned} \hat{\gamma}_s &= \varphi_s(\gamma), \\ \hat{H}_s &= \varphi_s(H_h), \end{aligned} \tag{15}$$

where, for any $p \in B(\gamma(s), \text{inj}(\gamma))$, $\varphi_s(p) = V_{\gamma(s)}^{-1} \circ \text{Exp}_{\gamma(s)}^{-1}(p)$ and $V_x : \mathbb{R}^D \rightarrow T_x \mathcal{M}$ is the basis isomorphism associated to any orthonormal basis $\{b_i\}_{i=1}^D$ of $T_x \mathcal{M}$, for any $x \in \mathcal{M}$.

The interpolation error in normal coordinates at $\gamma(s)$ is defined as $\hat{E}_s(\tau) = \hat{\gamma}_s(\tau) - \hat{H}_s(\tau)$ for every $\tau \in [t, t+h]$ and by construction satisfies

$$\begin{aligned} \hat{E}_s(t) &= 0, & \hat{E}_s(t+h) &= 0, \\ \frac{d}{d\tau} \hat{E}_s(\tau) \Big|_{\tau=t} &= 0, & \frac{d}{d\tau} \hat{E}_s(\tau) \Big|_{\tau=t+h} &= 0. \end{aligned}$$

By applying iteratively Rolle's theorem on the components $\hat{E}_{s,i}$ for each $i = 1, \dots, D$, we can show there exists $\xi_i \in [t, t+h]$ such that

$$|\hat{E}_{s,i}(\tau)| \leq \frac{|\hat{E}_{s,i}^{(4)}(\xi_i)|}{4!} h^4,$$

where the exponent in parentheses indicates the order of differentiation. Therefore, for any $s \in [t, t+h]$ we can bound the norm of the interpolation error as follows:

$$\begin{aligned} \|\hat{E}_s(\tau)\|_2 &\leq \frac{h^4}{4!} \left(\sum_{i=1}^D |\hat{E}_{s,i}^{(4)}(\xi_i)|^2 \right)^{1/2} \\ &\leq \frac{h^4}{4!} \sqrt{D} \max_{i=1, \dots, D} |\hat{E}_{s,i}^{(4)}(\xi_i)| \\ &\leq \frac{h^4}{4!} \sqrt{D} \max_{i=1, \dots, D} \|\hat{E}_s^{(4)}(\xi_i)\|_2 \\ &\leq \frac{h^4}{4!} \sqrt{D} \max_{\xi \in [t, t+h]} \|\hat{E}_s^{(4)}(\xi)\|_2. \end{aligned}$$

An important property of normal coordinates is that radial directions map to length-minimizing geodesics, thus $d(\gamma(\tau), H(\tau)) = \|V_{\gamma(\tau)} \hat{E}_\tau(\tau)\|_{\gamma(\tau)} = \|\hat{E}_\tau(\tau)\|_2$. So we can say

$$\begin{aligned} d(\gamma(\tau), H(\tau)) &\leq \frac{h^4}{4!} \sqrt{D} \max_{s, \xi \in [t, t+h]} \|\hat{E}_s^{(4)}(\xi)\|_2 \\ &\leq \frac{h^4}{4!} \sqrt{D} \max_{s, \xi \in [t, t+h]} \left\{ \|\hat{\gamma}_s^{(4)}(\xi)\|_2 + \|\hat{H}_s^{(4)}(\xi)\|_2 \right\} \end{aligned}$$

By the smoothness of the exponential map and its inverse, applying the chain rule to (15) gives an expression for $\hat{\gamma}_s^{(4)}$ and $\hat{H}_s^{(4)}$ respectively as the sum of contributions of the form

$$D^k \text{Exp}_{\gamma(s)}^{-1}(\gamma(\xi)) \left[\frac{D^{i_1} \gamma(\xi)}{d\xi^{i_1}}, \dots, \frac{D^{i_k} \gamma(\xi)}{d\xi^{i_k}} \right]$$

and

$$D^k \text{Exp}_{\gamma(s)}^{-1}(H_h(\xi)) \left[\frac{D^{i_1} H_h(\xi)}{d\xi^{i_1}}, \dots, \frac{D^{i_k} H_h(\xi)}{d\xi^{i_k}} \right]$$

with $k \in \{1, 2, 3, 4\}$ and $i_j \geq 0$ such that $i_1 + \dots + i_k = 4$ and where $D^k \text{Exp}_{\gamma(s)}^{-1}(\cdot)$ is the multilinear operator associated to the differential of order k . Then, the norm of each term is bounded by a constant independent of h (the maximum of the multilinear operator norms on the curve image) multiplied by the Lipschitz constant of the curve γ , the suprema of the norms of its higher order covariant derivatives and, provided $h < h_2$, the constants given by assumption (14). In summary, this produces a constant $\kappa > 0$ such that for any $h < \bar{h} := \min\{h_2, h_4\}$ and any $t \in [0, 1 - h]$ we have

$$\max_{\tau \in [t, t+h]} d(\gamma(\tau), H_h(\tau)) < \kappa h^4.$$

□

□

5 Numerical experiments

The following section is dedicated to numerical experiments illustrating the RH interpolation method, summarized in Algorithms 1 and 2. All experiments have been carried out in Matlab 2019b leveraging the differential geometry tools of the Manopt library [BMAS14] on a laptop computer with Intel i7 CPU (1.8GHz with single-thread mode) with 8GB of RAM, 1MB of L2 cache and 8MB of L3 cache.

5.1 Manifolds and retractions of interest

Let us briefly introduce the manifolds and retractions used in our experiments.

5.1.1 Stiefel manifold

The set of column orthogonal matrices of size $n \times k$ is a manifold of dimension $nk - \frac{k(k+1)}{2}$ that is commonly known as the (compact) Stiefel manifold and denoted by

$$\text{St}(n, k) := \left\{ X \in \mathbb{R}^{n \times k} : X^\top X = I_{k \times k} \right\}.$$

We endow the manifold with the Riemannian submanifold structure, i.e. by inducing on each tangent space $T_X \text{St}(n, k)$ the standard inner product on $\mathbb{R}^{n \times k}$. An exhaustive description of this structure can be found in [Bou23, §7.3] or [EAS99, §2.2]. On the Stiefel manifold we are aware of two retractions for which the inverse retraction can be conveniently computed. Given $X \in \text{St}(n, k)$ and $V \in T_X \text{St}(n, k)$ we define:

- the Q-factor retraction [Bou23, §7.3]:

$$R_X^Q(V) = \text{qf}(X + V)$$

where $\text{qf}(A) = Q \in \mathbb{R}^{n \times k}$ such that $A = QR$ is the unique (thin) QR decomposition of A . The uniqueness is guaranteed if A has full rank (which is the case for $X + V$) and if we enforce the diagonal entries of R to be positive. A procedure to compute the inverse Q-factor retraction is proposed in [KFT13, Algorithm 1] and consists of solving a linear matrix equation for an upper triangular matrix.

- the P-factor retraction [AM12, §3.3]:

$$R_X^P(V) = \text{pf}(X + V)$$

where $\text{pf}(A) = P$ such that $A = PS$ is the unique polar decomposition of the matrix A . The polar decomposition can be obtained from the SVD of the matrix. An algorithm to compute the inverse P-factor retraction is proposed in [KFT13, Algorithm 2] and requires solving a Lyapunov matrix equation.

5.1.2 Fixed-rank manifold

The set of $m \times n$ matrices of rank $k \leq \min\{m, n\}$ denoted by

$$\mathcal{M}_k := \{X \in \mathbb{R}^{m \times n} : \text{rank}(X) = k\}$$

is a manifold of dimension $(m + n - k)k$ embedded in $\mathbb{R}^{m \times n}$ [Lee03, Example 8.14].

Among many equivalent parametrizations of this manifold, we choose to represent points of \mathcal{M}_k with their economy-sized SVD. The manifold can be made an embedded Riemannian submanifold of $\mathbb{R}^{m \times n}$ by inducing on each tangent space the inner product of $\mathbb{R}^{m \times n}$. We refer the reader to [Van13] [UV20] for details on the representation and geometry of the manifold.

Possibly the most frequently used retraction on the rank- k matrix manifold is the k -truncated SVD retraction. However, we are not aware of any procedure allowing to compute efficiently the corresponding inverse retraction. As highlighted by Absil and Malick [AM12], an alternative retraction for the fixed-rank matrix manifold is the so-called orthographic retraction. It consists of perturbing the point X in the ambient space as $X + V \in \mathbb{R}^{m \times n}$ and projecting back onto the manifold along vectors from the normal space of the starting point, see Figure 3. Formally this reads:

$$R_X : V \in T_X \mathcal{M}_k \mapsto \arg \min_{P \in (X + V + N_X \mathcal{M}_k) \cap \mathcal{M}_k} \|X + V - P\|_F^2.$$

A closed-form expression for the solution of this optimization problem can be found in [AO15, §3.2]. The major advantage of the orthographic retraction is that the inverse retraction is trivial. As illustrated by Figure 3, it is sufficient to project the ambient space difference onto the tangent space, i.e. ,

$$R_X^{-1}(Y) = \Pi_X(Y - X).$$

5.2 Academic examples

In the following sections, we illustrate the RH interpolation scheme on two problems arising from numerical linear algebra: the computation of a smooth QR decomposition and a smooth singular value decomposition for a given smooth matrix curve $t \in [a, b] \rightarrow A(t) \in \mathbb{R}^{m \times n}$. Assuming for the moment that these smooth decomposition exist and can be computed, the experimental setup is the following. We sample the decomposition and its first order derivative at uniformly spaced locations and interpolate this data with different manifold interpolation schemes. We then vary the sampling step size h and measure the maximum interpolation error with respect to the original smooth decomposition.

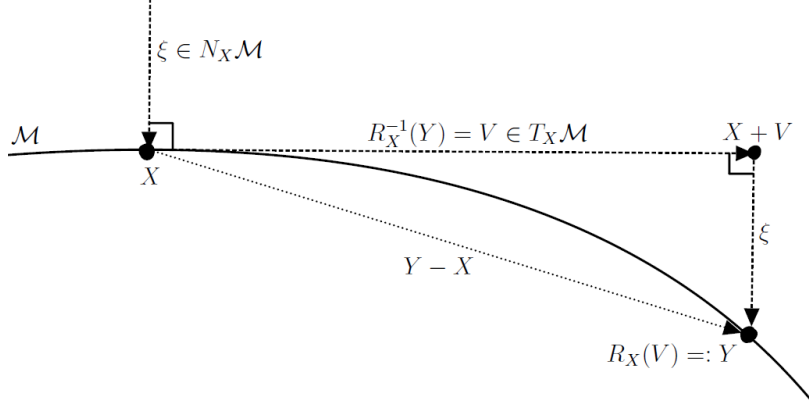


Figure 3: Orthographic retraction and its inverse.

5.2.1 Comparing with other retraction-based schemes

The RH method is compared with two other interpolation schemes that only use retractions. First, the analogous of the piecewise linear interpolant is defined as $L(t)|_{[t_i, t_{i+1}]} = c_0\left(\frac{t-t_i}{h}, p_i, p_{i+1}\right)$, where c_0 is the endpoint retraction curve defined in Definition 2. We then consider a naive piecewise Hermite interpolant that uses the same control points as the RH scheme but where only the endpoint curve c_0 is used as the building block for the generalized de Casteljau procedure. The resulting curve is then not expected to be continuously differentiable at the junctions.

5.2.2 Implementation details

To measure the error of an approximation $t \rightarrow \tilde{A}(t)$ to a matrix manifold curve $A(t)$, we consider the pointwise errors

$$\varepsilon_P(t) = \|A(t) - \tilde{A}(t)\|_F \quad \text{and} \quad \varepsilon_D(t) = \|\dot{A}(t) - \dot{\tilde{A}}(t)\|_F.$$

For convenience and the purpose of these experiments, we compute all required derivatives via centered finite differences:

$$\dot{A}(t) \simeq \Pi_{A(t)} \left(\frac{A(t + \Delta t) - A(t - \Delta t)}{2\Delta t} \right), \quad \Delta t = 10^{-5}. \quad (16)$$

Note that Theorem 17 uses the Riemannian distance to measure the interpolation error while we measure the error with the ambient space distance. It can be shown that if an embedded manifold is endowed with the induced metric, the Euclidean distance is locally equivalent to the Riemannian distance, see e.g. [AEM07, Appendix A].

5.2.3 Q-factor interpolation

For convenience, the example matrix curve we consider is the same as in [Zim20, §5.2]. It consists of the matrix polynomial

$$Y(t) = Y_0 + tY_1 + t^2Y_2 + t^3Y_3, \quad Y_i \in \mathbb{R}^{n \times k}, n = 500, k = 10, t \in [-1.1, 1.1], \quad (17)$$

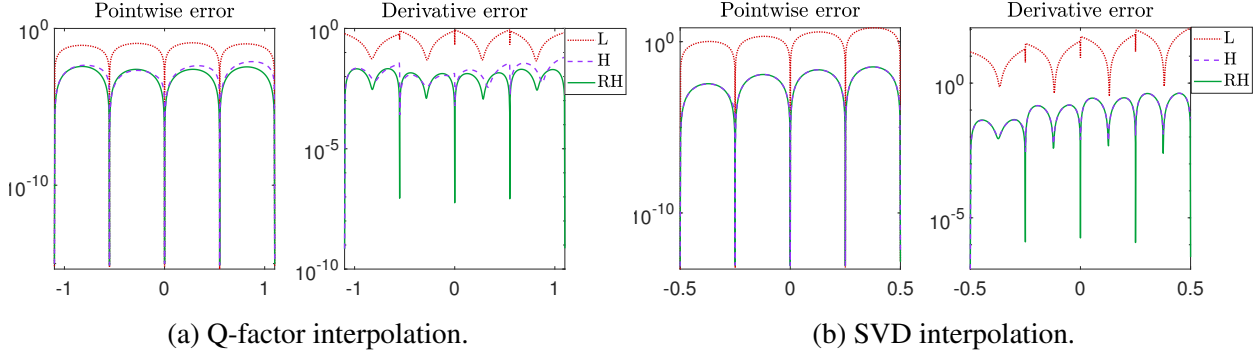


Figure 4: Interpolation error vs t for different retraction-based schemes: linear (L) and Hermite (H), as defined in Section 5.2.1, and the RH scheme.

Table 1: Average time per evaluation for the Q-factor and SVD interpolation experiments of Figure 4a and Figure 4b. In the last two lines we distinguish the naive and the optimized offline/online implementations of the RH scheme (see Algorithms 1 and 2).

Retraction used	Q-factor interpolation		SVD interpolation
	Q-factor	P-factor	Orthographic
Linear (L)	$1.524 \cdot 10^{-4}$	$2.049 \cdot 10^{-4}$	$1.710 \cdot 10^{-3}$
Hermite (H)	$1.540 \cdot 10^{-3}$	$1.596 \cdot 10^{-3}$	$1.147 \cdot 10^{-2}$
Retraction Hermite (RH)	$4.335 \cdot 10^{-3}$	$3.531 \cdot 10^{-3}$	$1.992 \cdot 10^{-2}$
Retraction Hermite (RH, optimized)	$2.226 \cdot 10^{-3}$	$2.188 \cdot 10^{-3}$	$1.558 \cdot 10^{-2}$

where the entries of the matrices Y_i are pseudo-randomly generated from uniform distributions on $[0, 1]$, $[0, 0.5]$, $[0, 0.5]$, $[0, 0.2]$ respectively. The matrix $Y(t)$ is generically full-rank for every $t \in [-1.1, 1.1]$ and is smooth, thus owing to [DE99, Proposition 2.3] there exist unique smooth curves $t \rightarrow Q(t) \in \text{St}(n, k)$ and $t \rightarrow R(t) \in \mathbb{R}^{k \times k}$ with positive diagonal entries, such that $Y(t) = Q(t)R(t)$. The positivity of the diagonal entries is explicitly enforced in the experiment. We focus on interpolating the curve $Q(t)$ on $\text{St}(n, k)$. At each sample location t_i we store $p_i = Q(t_i)$ and $v_i = \dot{Q}(t_i)$ obtained with (16).

In Figure 4a, we plot the pointwise and derivative error as a function of the curve parameter t when interpolating (17) with different schemes. While all schemes interpolate correctly the data points (left panel), only the RH scheme manages to match the derivative at sample points (right panel). Figure 5a illustrates the result of Theorem 17. Plotting the maximum pointwise interpolation error against the sampling step sizes h reveals the expected $O(h^4)$ trend for the RH scheme. Interestingly, as in the Euclidean case, the derivative error converges one order slower than the pointwise error. For these experiments we used the P-factor retraction, but analogous results are found with the Q-factor retraction. The difference between the two retractions is also negligible in terms of evaluation time as it can be seen from Table 1. These results also show that with the offline/online procedure proposed in Algorithms 1 and 2, the evaluation cost of the RH scheme is comparable with the one of other schemes. Note that, for a fair comparison, the other schemes have also been implemented in an offline/online fashion to minimize evaluation cost.

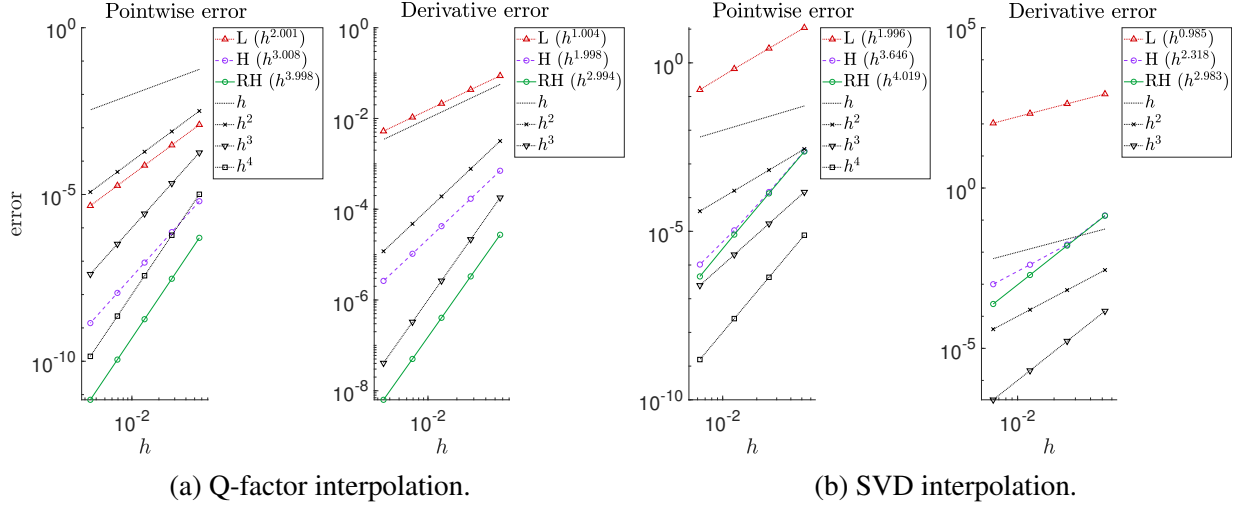


Figure 5: Interpolation error as a function of the sampling step size h for different retraction-based schemes: linear (L) and Hermite (H), as defined in Section 5.2.1, and the RH scheme.

5.2.4 SVD interpolation

We interpolate the singular value decomposition of a matrix curve of constant low rank. We consider $m = 10^4$, $n = 300$ and rank $r = 10$. We take

$$Y(t) = Y_0 + tY_1 + t^2Y_2 + t^3Y_3, \quad Y_i \in \mathbb{R}^{m \times r}$$

$$Z(t) = Z_0 + tZ_1 + t^2Z_2, \quad Z_i \in \mathbb{R}^{n \times r},$$

where the entries of Y_0, Z_0 and Y_1, Y_2, Y_3, Z_1, Z_2 are drawn from uniform random distributions on $[0, 1]$ and $[0, 0.5]$, respectively. Since the factors are generically of full rank, the curve

$$W(t) = Y(t)Z(t)^\top, \quad t \in [-0.5, 0.5] \quad (18)$$

is of rank r for every t . This example has also been taken from [Zim20, §5.3] together with the suggestion of Remark 6 from [Zim20] to ensure the smoothness of the computed SVD decomposition path $U(t)\Sigma(t)V(t)^\top = W(t)$. Note that this may cause negative values in the diagonal term.

The experimental results for the SVD path of (18) are reported in Figures 4b and 5b. The comments are analogous to the one we made for the Q-factor interpolation experiments: only the RH scheme manages to match the prescribed derivatives at the nodes thereby producing the expected $O(h^4)$ error convergence trend. For these experiments, the naive retraction-based Hermite interpolation scheme H produces a good approximation in terms of error, practically as good as the RH scheme. However, the curve H is not globally C^1 .

The computation time per evaluation for the different schemes is reported in Table 1. Interestingly, while for the Stiefel manifold, a naive implementation of the RH scheme is approximately two times slower than the offline/online approach, for the low-rank manifold, the non-optimized code is only 30% more expensive. We attribute this to the fact the inverse orthographic retraction is relatively cheap compared to the retraction and so the few inverse retractions spared by the offline/online implementation do not pay off as much.

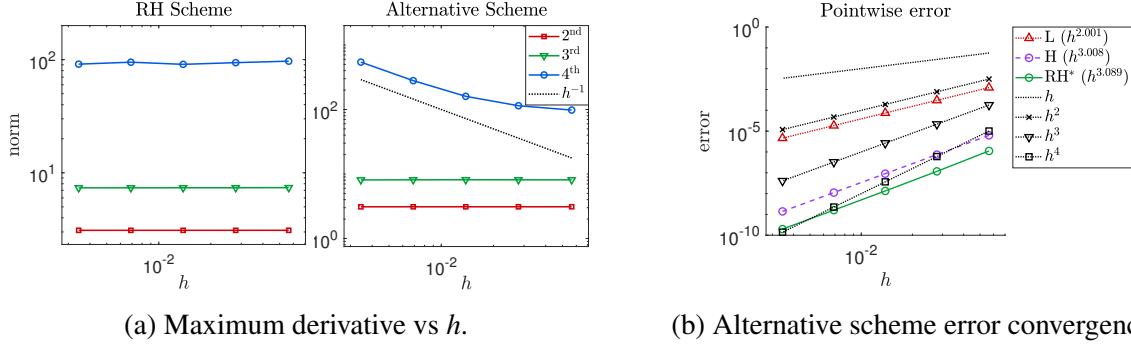


Figure 6: Experiments with an alternative interpolation scheme still satisfying Proposition 4 but failing to satisfy assumption (14).

5.2.5 The need for bounded derivatives

The fourth-order convergence achieved by the RH interpolation scheme was proved in Theorem 17 under the assumption that all derivatives up to order 4 of the interpolation curve remain bounded as $h \rightarrow 0$, see (14). As we now illustrate, this assumption can in fact not be removed. Recall that the RH interpolation scheme was built to satisfy Proposition 4 by making the choice (6). However, this choice was not unique and was motivated by the need to alleviate evaluation cost. It turns out that choice (6) is also important because it satisfies the bounded derivatives assumption (14). In Figure 6a we plot the maximum norm of the second, third and fourth order derivatives as a function of the sampling size h for the RH scheme and for an alternative scheme denoted RH* where choice (6) is modified with $r_1 = 0$ instead of $r_1 = 1/2$. It appears that unlike the RH scheme, the RH* scheme features a fourth derivative diverging as $O(h^{-1})$. Despite producing a continuously differentiable curve which interpolates the derivatives, the alternative scheme loses one order of accuracy as can be seen from Figure 6b. These experiments were conducted on the Q-factor interpolation of (17) on the Stiefel manifold but analogous results were found on the SVD interpolation instance.

Among the admissible choice determined by Proposition 4, the choice (6) is not the only one satisfying assumption (14). For instance, for any choice of $r_1 \in [0, 1]$ if we take $r_{01}(s, t) = (1 - r_1)t$, $r_{12}(s, t) = (1 - r_1) + r_1t$ and $r_{012}(u, s, t) = t$ we still achieve $O(h^4)$ error convergence. However, the evaluation cost of such schemes is higher and among those that we could find, choice (6) was the cheapest as its evaluation requires the least number of retraction and inverse retractions. The relationship between the choice of these functions and the fourth derivative of the scheme is intricate and we could not establish an a priori criterion to discriminate between schemes satisfying (14) and those violating it.

5.3 Applications

In this section, we illustrate two possible applications of the RH interpolation scheme. We focus on applications involving the fixed-rank manifold as we believe they are the most relevant.

5.3.1 Riemannian continuation

As a first application, we propose an extension of the numerical continuation method for Riemannian optimization from [SK22]. This application considers the minimization of a scalar target function $f(x, \lambda)$ for $x \in \mathcal{M}$ smoothly parametrized by $\lambda \in [0, 1]$. For example, this is useful when the minimum is simple to obtain for $\lambda = 0$ and one successively finds the minimum for increasing values of λ until one reaches $\lambda = 1$, corresponding to the minimization problem of interest. Suppose one has computed solutions \dots, x_{k-1}, x_k at previous parameter instances $\dots, \lambda_{k-1}, \lambda_k$ the computation of x_{k+1} at $\lambda_{k+1} = \lambda_k + h_k$ proceeds in two steps. The prediction step aims to attain a relatively cheap, yet accurate approximation y_{k+1} . This is followed by a standard Riemannian optimization method, warm started with the excellent initial guess y_{k+1} . The prediction step of the continuation algorithm can be characterized by the so-called prediction order [SK22, Definition 3.2]. It captures how accurately the prediction approximates the solution to the next problem. Theorem 17 indicates that using the RH interpolation scheme in the prediction step produces a prediction order $p_{RH} = 4$ compared to $p_C = 1$ and $p_T = 2$ for the classical and tangential prediction schemes discussed in [SK22]. Choosing constant step size $h_k = h$ for every $k \geq 0$, and introducing the notation $\tau \mapsto H(\tau; \{p_0, v_0, \tau_0\}, \{p_1, v_1, \tau_1\})$ to indicate the RH interpolant passing through p_i with velocity v_i at $\tau = \tau_i$, for $i = 0, 1$, we define the RH prediction step as

$$y_{k+1} = \begin{cases} R_{x_k}(ht_k) & k = 0, \\ H(2h; \{x_{k-1}, t_{k-1}, 0\}, \{x_k, t_k, h\}), & k \geq 1, \end{cases}$$

For $k = 0$, this is standard tangential prediction and, for $k \geq 1$, we employ a RH interpolant and to provide an initial guess to the next problem. Note that the RH interpolant itself is constructed on the interval $[0, h]$ as specified by Corollary 7. Yet, provided the retractions used in the procedure remain well-defined, we can evaluate it outside of this interval, in particular at $\tau = 2h$. This requires evaluating the elementary endpoint curves of the de Casteljau algorithm appearing in the lines 4 to 9 of Algorithm 2 outside the interval $[0, 1]$.

The RH prediction-correction continuation algorithm with fixed step size is applied to the same low-rank matrix completion problem considered in [SK22, §5]. We fix the number of steps to $N_{\text{steps}} = 5$, use the Riemannian Trust Regions (RTR) algorithm as a corrector and vary the prediction scheme. We report in Table 2 a comparison of the computational effort required to solve the problem with each scheme. There are two factors that determine the performance of the algorithm. First, the more ill-conditioned the final optimization problem is, the more the last RTR correction will encounter stagnation. Second, the more the underlying solution curve to the family of optimization problem is smooth, the more tangential and RH prediction will pay off. In fact, high prediction order will be achieved only when the underlying solution curve to the family of optimization problems is sufficiently smooth. Partly due to the choice of the homotopy, the solution curve often exhibited discontinuities thereby undermining the efficiency of tangential and RH prediction. Because of this, these two schemes were on average slower than classical prediction. However, when the underlying solution curve happens to be smooth, e.g. for the instance of Figure 7, the RH prediction benefits the increased prediction accuracy. As can be seen from the computed medians for computation time and total RTR iteration count, the RH can significantly reduce the computational effort compared to classical and tangential prediction.

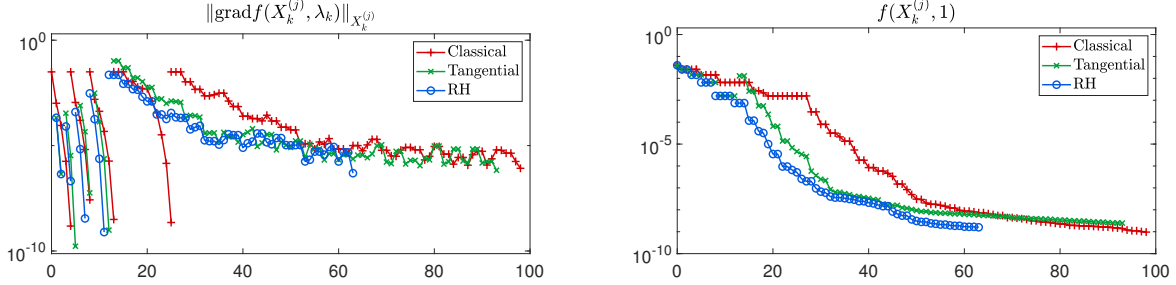


Figure 7: RH continuation algorithm on a favorable instance of matrix completion. Left: Riemannian gradient of the sequence of problems versus total iteration count. Right: objective function value of the final optimization problem versus total iteration count.

Table 2: Performance statistics of the Riemannian continuation algorithm for three different prediction schemes over 100 randomly generated instances of the matrix completion problem.

	Time (s)			Correction steps (RTR)		
	Mean	Median	Std. dev.	Mean	Median	Std. dev.
Classical	3.512	3.435	4.035	59.56	60	20.10
Tangential	7.919	4.706	6.735	69.95	53	66.16
RH	3.770	2.588	9.159	48.72	45	79.69

5.3.2 Dynamical-low-rank approximation interpolation

Dynamical low-rank approximation [KL07] (DLRA) is a numerical integration technique for solving a matrix differential equation of the form

$$\dot{Y} = F(Y, t), \quad Y(0) = Y_0, \quad Y(t) \in \mathbb{R}^{m \times n}, \quad t \in [0, t_{\text{end}}]. \quad (19)$$

Such equations arise, for example, from the structured discretization of two-dimensional partial differential equations. DLRA assumes that $Y(t)$ admits, for every t , an accurate rank- k approximation with $k \ll \min\{m, n\}$. In particular, this allows one to replace Y_0 by its best rank- k approximation \tilde{Y}_0 (using the singular value decomposition). Letting \mathcal{M}_k denote the manifold of rank- k matrices, one replaces the dynamics (19) by $\dot{\tilde{Y}} = \Pi_{\tilde{Y}}(F(\tilde{Y}, t))$, where $\Pi_{\tilde{Y}}$ denotes the orthogonal projection onto the tangent space $T_{\tilde{Y}}\mathcal{M}_k$, to ensure that $\tilde{Y}(t)$ remains on \mathcal{M}_k . This can significantly reduce the computational cost and memory requirements for numerical integration. In practice, some care is required in order to integrate the reduced differential equation on the manifold accurately and efficiently; see, e.g., [CL22]. Such an integrator returns a sequence $\{\tilde{Y}_i\}_{i=0}^{N_t} \subset \mathcal{M}_k$, such that $\tilde{Y}_i \simeq Y(t_i)$, the solution at time t_i of the matrix differential equation. During the numerical integration, for each \tilde{Y}_i we can store the best approximation of the vector $F(Y_i, t_i)$ on the tangent space $T_{\tilde{Y}_i}\mathcal{M}_k$, obtained as $\tilde{V}_i := \Pi_{\tilde{Y}_i}(F(\tilde{Y}_i, t_i))$. Then, the collection of triplets $\{(\tilde{Y}_i, \tilde{V}_i, t_i)\}_{i=0}^{N_t}$ can be fed to our RH interpolation scheme to obtain a continuously differentiable curve on \mathcal{M}_k that approximates the best rank k solution for every time t . Given the high accuracy of the interpolation scheme, one can expect that it is sufficient to interpolate a small fraction of the time samples to obtain a satisfactory approximation of the full solution curve.

We tested this hypothesis on the test case of [KEC23, §7.1] for which the DLRA integrator is the so-called unconventional time integrator [CL22], which features improved stability properties

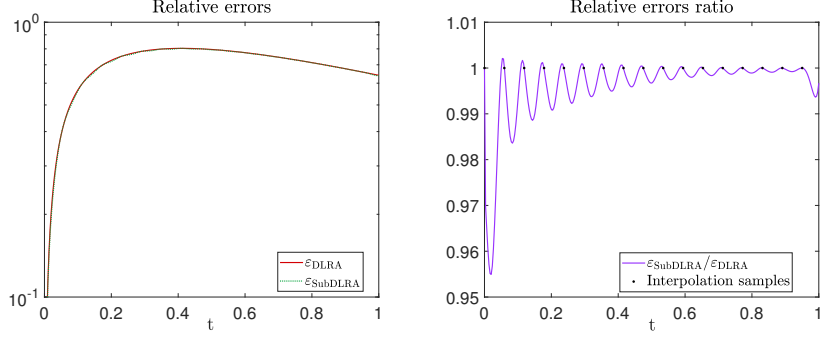


Figure 8: Relative error with reference solution of the interpolation of DLRA samples. The error ϵ_{DLRA} corresponds to interpolating all samples whereas $\epsilon_{\text{SubDLRA}}$ only 1 out of 20 samples.

compared to the matrix-projector splitting integrator. For conciseness, we refer the reader to these two references for details on the radiation transport equation at hand and on the numerical integrator. The parameters for the experiments are the same as in [KEC23, §7.1]: the integration is done on $\mathcal{M}_k \subset \mathbb{R}^{m \times n}$ with $m = 800$, $n = 100$ and $k = 15$. The only difference is that we turn off the rank adaptivity option of the integrator since we want the initial condition and all iterates to remain on \mathcal{M}_k . In order to obtain a rank 15 initial condition, we run the rank adaptive version starting from the rank 1 initial condition used in [KEC23, §7.1] and store the first sample of rank 15. From this initial condition, we run the unconventional DLRA integrator with a step size $\Delta t = 3 \times 10^{-3}$ for N_t steps up to $T = 1$. This yields $\{\tilde{Y}_i\}_{i=0}^{N_t} \subset \mathcal{M}_k$. We then obtain a reference solution by performing a forward Euler integration of the ODE in $\mathbb{R}^{m \times n}$ with a step size 20 times smaller than the unconventional integrator. These samples are then projected to \mathcal{M}_k with the k -truncated SVD, and we denote them $\{Y_j\}_{j=0}^{20N_t}$. Finally, we assemble three RH interpolants:

$$\begin{aligned}\tilde{Y}(t) &= H\left(t; \{(\tilde{Y}_i, \tilde{V}_i, t_i)\}_{i=0}^{N_t}\right), \\ \hat{Y}(t) &= H\left(t; \{(\tilde{Y}_{20l}, \tilde{V}_{20l}, t_{20l})\}_{l=0}^{\lfloor N_t/20 \rfloor}\right), \\ Y(t) &= H\left(t; \{(Y_j, V_j, t_j)\}_{j=0}^{20N_t}\right)\end{aligned}$$

where tangent vectors \tilde{V}_i and V_i are obtained as explained previously. The curve \hat{Y} interpolates one every 20 samples of the DLRA solution, so roughly 5% of the integrator's output. Yet, as can be seen from Figure 8, the relative errors

$$\epsilon_{\text{DLRA}}(t) = \frac{\|\tilde{Y}(t) - Y(t)\|_F}{\|Y(t)\|_F}, \quad \epsilon_{\text{SubDLRA}}(t) = \frac{\|\hat{Y}(t) - Y(t)\|_F}{\|Y(t)\|_F},$$

are almost identical. Surprisingly, the sub-sampled interpolation curve \hat{Y} can be more precise, though from a negligible amount. The real advantage comes in terms of storage requirements: the information needed to evaluate the sub-sampled interpolation curve \hat{Y} occupies 20 times less memory than the information for the curve \tilde{Y} and approximately 4 times less storage than the full collection of samples $\{\tilde{Y}_i\}_{i=0}^{N_t}$. This application of RH interpolation can be thought as a compression post-processing that enhances the portability of DLRA solutions.

6 Conclusion

We have proposed a manifold interpolation technique to address Hermite interpolation of manifold curves. The method is general enough to be applicable to every manifold for which a retraction/inverse retraction pair is available, thereby avoiding the need for Riemannian exponential and logarithmic maps used by other interpolation schemes that take into account derivative information.

The novel notion of retraction-convex sets ensures the well-posedness of the method, provided that the interpolation data is sufficiently close. Theorem 17 generalizes to our scheme the classical interpolation error convergence result for polynomial Hermite interpolation in Euclidean spaces. The predicted $O(h^4)$ convergence trend has also been experimentally observed for academic interpolation problems on the Stiefel manifold and the fixed-rank matrix manifold. The high order accuracy of the method allowed us to propose an improvement to the prediction-correction Riemannian continuation algorithm of [SK22] and to suggest a strategy to compress the output of dynamical low-rank matrix integrators.

Just like curve interpolation is a basic tool in many context of numerical analysis, we believe the RH interpolation scheme could serve as a building block for many other numerical methods on manifolds, for example the numerical integration of manifold ODEs.

Acknowledgements The authors would like to thank Ralf Zimmerman for helpful discussions on the topic and Gianluca Ceruti for suggesting the DLRA application as well as providing the code for the unconventional integrator from [KEC23]. The authors thank the reviewer for very helpful remarks.

Conflicts of interest The authors have no conflicts of interest to declare that are relevant to the content of this article.

References

- [AAM14] P.-A. Absil, L. Amodei, and G. Meyer. Two Newton methods on the manifold of fixed-rank matrices endowed with Riemannian quotient geometries. *Comput. Statist.*, 29(3-4):569–590, 2014.
- [AEM07] D. Attali, H. Edelsbrunner, and Y. Mileyko. Weak witnesses for Delaunay triangulations of submanifolds. In *Proceedings of the 2007 ACM Symposium on Solid and Physical Modeling, SPM '07*, page 143–150, New York, NY, USA, 2007. Association for Computing Machinery.
- [AM12] P.-A. Absil and J. Malick. Projection-like retractions on matrix manifolds. *SIAM J. Optim.*, 22(1):135–158, 2012.
- [AMS08] P.-A. Absil, R. Mahony, and R. Sepulchre. *Optimization algorithms on matrix manifolds*. Princeton University Press, Princeton, NJ, 2008.
- [Ams10] D. Amsallem. *Interpolation on Manifolds of Cfd-Based Fluid and Finite Element-Based Structural Reduced-Order Models for On-Line Aeroelastic Predictions*. ProQuest LLC, Ann Arbor, MI, 2010. Thesis (Ph.D.)–Stanford University.

- [AO15] P.-A. Absil and I. V. Oseledets. Low-rank retractions: a survey and new results. *Comput. Optim. Appl.*, 62(1):5–29, 2015.
- [BCC21] A. Bloch, M. Camarinha, and L. J. Colombo. Dynamic interpolation for obstacle avoidance on Riemannian manifolds. *Internat. J. Control*, 94(3):588–600, 2021.
- [BKSL17] J. Batista, K. Krakowski, and F. Silva Leite. Exploring quasi-geodesics on stiefel manifolds in order to smooth interpolate between domains. In *2017 IEEE 56th Annual Conference on Decision and Control (CDC)*, pages 6395–6402, 2017.
- [BMAS14] N. Boumal, B. Mishra, P.-A. Absil, and R. Sepulchre. Manopt, a Matlab toolbox for optimization on manifolds. *Journal of Machine Learning Research*, 15(42):1455–1459, 2014.
- [Bou23] Nicolas Boumal. *An introduction to optimization on smooth manifolds*. Cambridge University Press, Cambridge, 2023.
- [CEM06] R. D. Canary, D. Epstein, and A. Marden, editors. *Fundamentals of hyperbolic geometry: selected expositions*, volume 328 of *London Mathematical Society Lecture Note Series*. Cambridge University Press, Cambridge, 2006.
- [CKSL99] P. Crouch, G. Kun, and F. Silva Leite. The de Casteljau algorithm on Lie groups and spheres. *J. Dynam. Control Systems*, 5(3):397–429, 1999.
- [CL22] G. Ceruti and C. Lubich. An unconventional robust integrator for dynamical low-rank approximation. *BIT*, 62(1):23–44, 2022.
- [CSLC95] M. Camarinha, F. Silva Leite, and P. Crouch. Splines of class C^k on non-Euclidean spaces. *IMA J. Math. Control Inform.*, 12(4):399–410, 1995.
- [dC59] P. de Casteljau. Outillages méthode calcul. Technical report, André Citroën Automobiles, Paris, 1959.
- [dC92] M. P. do Carmo. *Riemannian geometry*. Mathematics: Theory & Applications. Birkhäuser Boston, Inc., Boston, MA, 1992.
- [DE99] L. Dieci and T. Eirola. On smooth decompositions of matrices. *SIAM J. Matrix Anal. Appl.*, 20(3):800–819, 1999.
- [EAS99] A. Edelman, T. A. Arias, and S. T. Smith. The geometry of algorithms with orthogonality constraints. *SIAM J. Matrix Anal. Appl.*, 20(2):303–353, 1999.
- [Far02] G. Farin. *Curves and Surfaces for CAGD: A Practical Guide*. Computer graphics and geometric modeling. Elsevier Science, 2002.
- [GHL04] S. Gallot, D. Hulin, and J. Lafontaine. *Riemannian geometry*. Universitext. Springer-Verlag, Berlin, third edition, 2004.

- [GSA14] P.-Y. Gousenbourger, C. Samir, and P.-A. Absil. Piecewise-Bézier C^1 interpolation on Riemannian manifolds with application to 2D shape morphing. In *Proceedings - International Conference on Pattern Recognition*, pages 4086–4091, 08 2014.
- [HAG15] W. Huang, P.-A. Absil, and K. A. Gallivan. A Riemannian symmetric rank-one trust-region method. *Math. Program.*, 150(2, Ser. A):179–216, 2015.
- [KDLS21] K.-R. Kim, I. L. Dryden, H. Le, and K. E. Severn. Smoothing splines on Riemannian manifolds, with applications to 3D shape space. *J. R. Stat. Soc. Ser. B. Stat. Methodol.*, 83(1):108–132, 2021.
- [KEC23] Jonas Kusch, Lukas Einkemmer, and Gianluca Ceruti. On the stability of robust dynamical low-rank approximations for hyperbolic problems. *SIAM J. Sci. Comput.*, 45(1):A1–A24, 2023.
- [KFT13] T. Kaneko, S. Fiori, and T. Tanaka. Empirical arithmetic averaging over the compact Stiefel manifold. *IEEE Trans. Signal Process.*, 61(4):883–894, 2013.
- [KL07] O. Koch and C. Lubich. Dynamical low-rank approximation. *SIAM J. Matrix Anal. Appl.*, 29(2):434–454, 2007.
- [KMSLB17] K. A. Krakowski, L. Machado, F. Silva Leite, and J. Batista. A modified Casteljau algorithm to solve interpolation problems on Stiefel manifolds. *J. Comput. Appl. Math.*, 311:84–99, 2017.
- [Lee03] J. M. Lee. *Introduction to smooth manifolds*, volume 218 of *Graduate Texts in Mathematics*. Springer-Verlag, New York, 2003.
- [Lee18] J. M. Lee. *Introduction to Riemannian manifolds*, volume 176 of *Graduate Texts in Mathematics*. Springer, Cham, 2018.
- [MMH⁺22] A. Musolas, E. Massart, J. M. Hendrickx, P.-A. Absil, and Y. Marzouk. Low-rank multi-parametric covariance identification. *BIT*, 62(1):221–249, 2022.
- [NYP13] E. Nava-Yazdani and K. Polthier. De Casteljau’s algorithm on manifolds. *Comput. Aided Geom. Design*, 30(7):722–732, 2013.
- [PN07] T. Popiel and L. Noakes. Bézier curves and C^2 interpolation in Riemannian manifolds. *J. Approx. Theory*, 148(2):111–127, 2007.
- [PR95] F. C. Park and B. Ravani. Bézier curves on Riemannian manifolds and Lie groups with kinematics applications. *Journal of Mechanical Design*, 117(1):36–40, 03 1995.
- [QSS07] A. Quarteroni, R. Sacco, and F. Saleri. *Numerical mathematics*, volume 37 of *Texts in Applied Mathematics*. Springer-Verlag, Berlin, second edition, 2007.
- [RSLJ05] R. C. Rodrigues, F. Silva Leite, and J. Jakubiak. A new geometric algorithm to generate smooth interpolating curves on Riemannian manifolds. *LMS J. Comput. Math.*, 8:251–266, 2005.

- [RW12] W. Ring and B. Wirth. Optimization methods on Riemannian manifolds and their application to shape space. *SIAM J. Optim.*, 22(2):596–627, 2012.
- [SK22] A. Séguin and D. Kressner. Continuation methods for Riemannian optimization. *SIAM J. Optim.*, 32(2):1069–1093, 2022.
- [UV20] André Uschmajew and Bart Vandereycken. Geometric methods on low-rank matrix and tensor manifolds. In *Handbook of variational methods for nonlinear geometric data*, pages 261–313. Springer, Cham, 2020.
- [Van13] B. Vandereycken. Low-rank matrix completion by Riemannian optimization. *SIAM J. Optim.*, 23(2):1214–1236, 2013.
- [ZB22] R. Zimmermann and R. Bergmann. Multivariate Hermite interpolation of manifold-valued data. *arXiv preprint arXiv:2212.07281*, 2022.
- [Zim17] R. Zimmermann. A matrix-algebraic algorithm for the Riemannian logarithm on the Stiefel manifold under the canonical metric. *SIAM J. Matrix Anal. Appl.*, 38(2):322–342, 2017.
- [Zim20] R. Zimmermann. Hermite interpolation and data processing errors on Riemannian matrix manifolds. *SIAM J. Sci. Comput.*, 42(5):A2593–A2619, 2020.
- [ZN19] E. Zhang and L. Noakes. The cubic de Casteljau construction and Riemannian cubics. *Comput. Aided Geom. Design*, 75:101789, 16, 2019.

A Lipschitz continuity of the retraction

In this section, we establish the Lipschitz continuity properties of retractions stated in Section 4.1 and used in Appendix B below.

Recall that Proposition 8 yields a suitable domain $\mathcal{T} \subset T\mathcal{M}$ of invertibility of the retraction. We set $\mathcal{I}_x := \pi_{T_x\mathcal{M}}(\mathcal{T})$ and $\mathcal{I}_x := R_x(\mathcal{I}_x)$ for $x \in \mathcal{M}$. For any $\varepsilon \in (0, 1)$ we define

$$\mathcal{T}^\varepsilon := \{(x, v) \in T\mathcal{M} : \|v\|_x < \varepsilon\Delta(x)\},$$

an open set that satisfies $\overline{\mathcal{T}^\varepsilon} \subset \mathcal{T}$. Similarly, we set $\mathcal{I}_x^\varepsilon := \pi_{T_x\mathcal{M}}(\mathcal{T}^\varepsilon)$ and $\mathcal{I}_x^\varepsilon = R_x(\mathcal{I}_x^\varepsilon)$.

We consider differentials of the retraction and inverse retraction with respect to their arguments. Given $x \in \mathcal{M}$, $u \in \mathcal{I}_x$, $v \in T_x\mathcal{M}$, $y \in \mathcal{I}_x$ and $w \in T_y\mathcal{M}$ we denote

$$\begin{aligned} D_1R_x(u)[v] &= \left. \frac{d}{dt}R_{\sigma_{x,v}(t)}(u) \right|_{t=0} \in T_{R_x(u)}\mathcal{M}, \\ D_2R_x(u)[v] &= \left. \frac{d}{dt}R_x(u + tv) \right|_{t=0} \in T_{R_x(u)}\mathcal{M}, \\ D_1R_x^{-1}(y)[v] &= \left. \frac{d}{dt}R_{\sigma_{x,v}(t)}^{-1}(y) \right|_{t=0} \in T_x\mathcal{M}, \\ D_2R_x^{-1}(y)[w] &= \left. \frac{d}{dt}R_x^{-1}(\sigma_{y,w}(t)) \right|_{t=0} \in T_x\mathcal{M}, \end{aligned}$$

where $\sigma_{x,v}$ is any continuously differentiable manifold curve defined in a neighborhood of $t = 0$ such that $\sigma_{x,v}(0) = x$, $\dot{\sigma}_{x,v}(0) = v$.

Proposition 21. Consider arbitrary $\varepsilon \in (0, 1)$. For any $x \in \mathcal{M}$, there exist positive constants $L_1(x, \varepsilon)$, $M_1(x, \varepsilon)$, $L_2(x, \varepsilon)$ and $M_2(x, \varepsilon)$ such that the retraction R satisfies

- (i) $\|D_1 R_x(u)[v]\|_{R_x(u)} \leq L_1(x, \varepsilon) \|v\|_x$ for every $u \in \mathcal{I}_x^\varepsilon$ and $v \in T_x \mathcal{M}$
- (ii) $\|D_2 R_x(u)[v]\|_{R_x(u)} \leq L_2(x, \varepsilon) \|v\|_x$ for every $u \in \mathcal{I}_x^\varepsilon$ and $v \in T_u T_x \mathcal{M} \simeq T_x \mathcal{M}$,
- (iii) $\|D_1 R_x^{-1}(y)[v]\|_x \leq M_1(x, \varepsilon) \|v\|_x$ for every $y \in \mathcal{I}_x^\varepsilon$ and $v \in T_x \mathcal{M}$,
- (iv) $\|D_2 R_x^{-1}(y)[v]\|_x \leq M_2(x, \varepsilon) \|v\|_y$ for every $y \in \mathcal{I}_x^\varepsilon$ and $v \in T_y \mathcal{M}$.

Proof. The result follows from the smoothness of the retraction and its inverse. The Lipschitz constants are found by taking the maxima of the operator norm for the differentials of the retraction on the compact set $\overline{\mathcal{I}_x^\varepsilon}$ and of the inverse retraction on the compact set $\overline{\mathcal{I}_x^\varepsilon}$. \square \square

For simplicity of exposition, a particular choice $\varepsilon = 1/3$ is considered in Lemma 14. Note however that the result (and the upcoming proof) hold for any $\varepsilon \in (0, \frac{1}{2})$

Proof. (of Lemma 14)

- (i) Consider any $x \in \mathcal{M}$, $u, v \in \mathcal{I}_x^{1/3}$ and define a manifold curve joining $R_x(u)$ and $R_x(v)$ as $\delta(\tau) := R_x(u + \tau(v - u))$. It is well-defined by the convexity of $\mathcal{I}_x^{1/3}$. By definition, the manifold distance between $R_x(u)$ and $R_x(v)$ is bounded by the length $L(\delta)$ of the curve δ . Thus we have

$$\begin{aligned} d(R_x(u), R_x(v)) &\leq L(\delta) = \int_0^1 \|D_2 R_x(u + \tau(v - u))[v - u]\|_{\delta(\tau)} d\tau \\ &\leq L_2(x, 1/3) \|v - u\|_x, \end{aligned}$$

where the final inequality follows from Proposition 21-(ii). Hence $L_R(x) = L_2(x, 1/3)$.

- (ii) Consider $y, z \in \mathcal{I}_x^{1/3}$. Since \mathcal{M} is connected, by definition of the distance function we know there exists a sequence of piecewise smooth manifold curves $\gamma_k : [0, 1] \rightarrow \mathcal{M}$, $k \in \mathbb{N}$, such that

$$\gamma_k(0) = y, \quad \gamma_k(1) = z, \quad \forall k \in \mathbb{N}$$

and

$$\lim_{k \rightarrow \infty} L(\gamma_k) = \inf_{k \in \mathbb{N}} \{L(\gamma_k)\} = d(y, z).$$

If the image of the curve γ_k , is fully contained in $\mathcal{I}_x^{2/3}$, we can define the tangent space curve $q(t) := R_x^{-1}(\gamma_k(t))$ for every $t \in [0, 1]$ and deduce that

$$\begin{aligned} \|R_x^{-1}(y) - R_x^{-1}(z)\|_x &\leq \int_0^1 \|D_2 R_x^{-1}(\gamma_k(\tau))[\dot{\gamma}_k(\tau)]\|_x d\tau \\ &\leq M_2(x, 2/3) \int_0^1 \|\dot{\gamma}_k(\tau)\|_{\gamma_k(\tau)} d\tau, \\ &= M_2(x, 2/3) L(\gamma_k) \end{aligned}$$

If the image of the curve γ_k is not fully contained in $\mathcal{S}_x^{2/3}$, then let

$$t_1 = \inf \left\{ t \in [0, 1] : \gamma_k(t) \notin \mathcal{S}_x^{2/3} \right\},$$

$$t_2 = \sup \left\{ t \in [0, 1] : \gamma_k(t) \notin \mathcal{S}_x^{2/3} \right\}.$$

Therefore we can define the tangent space curve $q(t) = R_x^{-1}(\gamma_k(t))$ only for $t \in [0, t_1) \cup (t_2, 1]$. Since $y, z \in \mathcal{S}_x^{1/3}$, it follows that

$$\|R_x^{-1}(y) - R_x^{-1}(z)\|_x \leq 2\Delta(x)/3$$

Furthermore, the tangent space curve q traverses the tangent space spherical annulus of width $\Delta(x)/3$ back and forth, hence its length must exceed $2\Delta(x)/3$, i.e.

$$2/3\Delta(x) \leq \int_{[0, t_1) \cup (t_2, 1]} \|\dot{q}(\tau)\|_x d\tau.$$

Hence, we recover the same inequality as before

$$\begin{aligned} \|R_x^{-1}(y) - R_x^{-1}(z)\|_x &\leq \int_{[0, t_1) \cup (t_2, 1]} \|D_2 R_x^{-1}(\gamma_k(\tau)) [\dot{\gamma}_k(\tau)]\|_x d\tau, \\ &\leq M_2(x, 2/3) \int_{[0, t_1) \cup (t_2, 1]} \|\dot{\gamma}_k(\tau)\|_{\gamma_k(\tau)} d\tau, \\ &\leq M_2(x, 2/3)L(\gamma_k). \end{aligned}$$

We have shown that for every $k \in \mathbb{N}$

$$\|R_x^{-1}(y) - R_x^{-1}(z)\|_x \leq M_2(x, 2/3)L(\gamma_k).$$

Therefore the result remains true upon taking the infimum over $k \in \mathbb{N}$, which yields

$$\|R_x^{-1}(y) - R_x^{-1}(z)\|_x \leq M_2(x, 2/3)d(x, y)$$

as desired and shows $M_R(x) = M_2(x, 2/3)$.

□

□

The results of Corollary 15 requires to bound the local Lipschitz constant of the retraction on any compact set $K \subset \mathcal{M}$. The following more general result shows this is possible for all local Lipschitz constants of the retractions introduced in Proposition 21.

Proposition 22. *For every compact set $K \subset \mathcal{M}$ and every $\varepsilon \in (0, 1)$, inequalities of Proposition 21 hold for every $x \in K$ with finite strictly positive constants $L_1(K, \varepsilon)$, $L_2(K, \varepsilon)$, $M_1(K, \varepsilon)$, $M_2(K, \varepsilon)$ depending only on K .*

The proof of Proposition 22 is straightforward once the following result is established.

Lemma 23. *For every compact set $K \subset \mathcal{M}$ and every $\varepsilon \in (0, 1)$, the sets*

$$\overline{\mathcal{I}}_K^\varepsilon := \bigcup_{x \in K} \overline{\mathcal{I}}_x^\varepsilon \subset \mathcal{M}, \quad \overline{\mathcal{T}}_K^\varepsilon := \{(x, v) \in \mathcal{T} : x \in K, \|v\|_x \leq \varepsilon\Delta(x)\} \subset T\mathcal{M},$$

are compact sets.

Proof. We have that $E(\overline{\mathcal{T}}_K^\varepsilon) = K \times \overline{\mathcal{S}}_K^\varepsilon$, where E is the diffeomorphism of Proposition 8. Therefore, since K is compact, $\overline{\mathcal{T}}_K^\varepsilon$ is compact if and only if $\overline{\mathcal{S}}_K^\varepsilon$ is compact. Let us prove $\overline{\mathcal{T}}_K^\varepsilon$ is sequentially compact, equivalent to being compact by the assumed second countability of the manifold topology.

Consider any sequence $\{(x_n, v_n)\}_{n \in \mathbb{N}} \subset \overline{\mathcal{T}}_K^\varepsilon$. Then $\{x_n\}_{n \in \mathbb{N}} \subset K$ and so there exists a convergent subsequence $\{x_{n_k}\}_{k \in \mathbb{N}}$ such that $x_{n_k} \xrightarrow{k \rightarrow \infty} x \in K$. Then there exists $N > 0$ such that for every $k > N$, $x_{n_k} \in \mathcal{S}_x^\varepsilon$. Therefore the retraction curve $\sigma_k(\tau) = R_x(\tau R_x^{-1}(x_{n_k}))$ is well-defined for all $k > N$. Consider the parallel transport map along σ_k [Bou23, Definition 10.35] denoted $P_{1 \rightarrow 0}^{\sigma_k} : T_{x_{n_k}} \mathcal{M} \rightarrow T_x \mathcal{M}$. It is uniquely defined and is an isometry [Bou23, Proposition 10.36]. Let us define $w_k = P_{1 \rightarrow 0}^{\sigma_k} v_{n_k} \in T_x \mathcal{M}$. Then since $\|v_{n_k}\|_{x_{n_k}} \leq \varepsilon \Delta(x_{n_k})$ and $P_{1 \rightarrow 0}^{\sigma_k}$ is an isometry, then $\|w_k\|_x \leq \varepsilon \Delta(x_{n_k})$. By the continuity of Δ we know $\{\varepsilon \Delta(x_{n_k})\}_{k \in \mathbb{N}}$ is a convergent, hence bounded sequence. Therefore $\{w_k\}_{k \in \mathbb{N}} \subset T_x \mathcal{M}$ is a bounded sequence, and thus admits a convergent subsequence $\{w_{k_j}\}_{j \in \mathbb{N}}$ such that $w_{k_j} \xrightarrow{j \rightarrow \infty} w \in T_x \mathcal{M}$. But since $\|w_{k_j}\|_x \leq \varepsilon \Delta(x_{n_{k_j}})$, we have that $\|w\|_x \leq \varepsilon \Delta(x)$ and consequently that $(x, w) \in \overline{\mathcal{T}}_K^\varepsilon$. The standard Riemannian metric on the tangent bundle associated to any Riemannian manifold, also known as Sasaki metric [GHL04, p. 80], allows the definition of a distance function on the tangent bundle defined analogously to (1), see [CEM06, p. 240]. Then we have that

$$d\left((x, w), (x_{n_{k_j}}, v_{n_{k_j}})\right) \leq \sqrt{L(\sigma_k)^2 + \left\|w - P_{1 \rightarrow 0}^{\sigma_{k_j}} v_{n_{k_j}}\right\|_x}$$

Since the right-hand side converges to zero as $j \rightarrow +\infty$, this shows that $\{(x_{n_{k_j}}, v_{n_{k_j}})\}$ converges to $(x, w) \in \overline{\mathcal{T}}_K^\varepsilon$, concluding the proof. \square \square

Proof. (of Proposition 22) We know that the map E of Proposition 8 is a diffeomorphism on \mathcal{T} . Therefore, the differentials of the retraction on $\overline{\mathcal{T}}_K^\varepsilon$ and of the inverse retraction on $\overline{\mathcal{S}}_K^\varepsilon$ are continuous and have continuous operator norm. Since by Lemma 23 these sets are compact, the operator norm attains a (finite) maximum. The constants $L_1(K, \varepsilon)$, $L_2(K, \varepsilon)$, $M_1(K, \varepsilon)$, $M_2(K, \varepsilon)$ are obtained by maximizing $\|D_1 R\|_{\text{op}}$ and $\|D_2 R\|_{\text{op}}$ on $\overline{\mathcal{T}}_K^\varepsilon$ and $\|D_1 R^{-1}\|_{\text{op}}$ and $\|D_2 R^{-1}\|_{\text{op}}$ on $\overline{\mathcal{S}}_K^\varepsilon$, respectively. \square \square

B Proof of Lipschitz continuity of RH scheme independent of h

The proof of Lemma 19 leverages the Lipschitz continuity of the retraction discussed in Section 4.1 and detailed Appendix A. Therefore note that the following sections employ notations introduced at the beginning of Appendix A.

In this section, we first show the Lipschitz continuity of the r -endpoint retraction curve with respect to each of its arguments and then to all its arguments jointly. These preliminary results will be used in the proof of Lemma 19, reported in Appendix B.2.

B.1 Preliminary results

Lemma 24. *Let $\mathcal{U} \subset \mathcal{M}$ be retraction-convex such that*

$$\mathcal{U} \subset \mathcal{I}_z^{1/3}, \quad \forall z \in \mathcal{U}. \quad (20)$$

The exist positive constants L_t , L_r and L_{xy} depending on the retraction verifying:

$$(i) \quad d(c_r(t_1; x, y), c_r(t_2; x, y)) \leq L_t d(x, y) |t_1 - t_2|, \quad \forall x, y \in \mathcal{U}, \quad \forall r, t_1, t_2 \in [0, 1].$$

$$(ii) \quad d(c_{r_1}(t; x, y), c_{r_2}(t; x, y)) \leq L_r d(x, y) |r_1 - r_2|, \quad \forall x, y \in \mathcal{U}, \quad \forall r_1, r_2, t \in [0, 1].$$

$$(iii) \quad d(c_r(t; x_1, y_1), c_r(t; x_2, y_2)) \leq L_{xy}(d(x_1, x_2) + d(y_1, y_2)), \quad \forall x_1, x_2, y_1, y_2 \in \mathcal{U}, \quad \forall r, t \in [0, 1].$$

Proof. Given $x, y \in \mathcal{U}$ and $r, t \in [0, 1]$, first observe that (20) implies that the evaluation of $c_r(t; x, y)$ requires only the evaluation of the retraction on $\mathcal{I}_z^{1/3}$ and of the inverse retraction on $\mathcal{I}_z^{1/3}$ for several $z \in \mathcal{U}$. Pick any $z \in \mathcal{U}$, denote $K = \overline{\mathcal{I}_z^{1/3}}$ and consider the retraction's Lipschitz constants $L_1(K, 1/3)$, $L_2(K, 1/3)$, $M_1(K, 1/3)$ and $M_2(K, 1/3)$ as introduced in Proposition 22 and $L_R(K) = L_2(K, 1/3)$ and $M_R(K) = M_2(K, 2/3)$ introduced in Corollary 15. For conciseness, we simply denote

$$\begin{aligned} L_1 &= L_1(K, 1/3), & L_2 &= L_2(K, 1/3), \\ M_1 &= M_1(K, 1/3), & M_2 &= M_2(K, 2/3). \end{aligned}$$

and we use the results of Lemma 14 and Proposition 21 with these constants.

(i) Using Lemma 14 with the constants defined above

$$\begin{aligned} & d(c_r(t_1; x, y), c_r(t_2; x, y)) \\ &= d\left(R_{q(r)}\left(R_{q(r)}^{-1}(x) + t_1\left(R_{q(r)}^{-1}(y) - R_{q(r)}^{-1}(x)\right)\right), \right. \\ & \quad \left. R_{q(r)}\left(R_{q(r)}^{-1}(x) + t_2\left(R_{q(r)}^{-1}(y) - R_{q(r)}^{-1}(x)\right)\right)\right) \\ & \leq L_2 \|R_{q(r)}^{-1}(y) - R_{q(r)}^{-1}(x)\|_{q(r)} |t_1 - t_2| \\ & \leq L_2 M_2 d(x, y) |t_1 - t_2|. \end{aligned}$$

Therefore we can choose $L_t = L_2 M_2$.

(ii) The smooth curve $\delta(\tau) := c_{r(\tau)}(t; x, y)$, where $r(\tau) = (1 - \tau)r_1 + \tau r_2$, $\tau \in [0, 1]$, joins $c_{r_1}(t; x, y)$ and $c_{r_2}(t; x, y)$. Therefore we can bound

$$d(c_{r_1}(t; x, y), c_{r_2}(t; x, y)) \leq L(\delta) \leq \max_{\tau \in [0, 1]} \left\{ \left\| \dot{\delta}(\tau) \right\|_{\delta(\tau)} \right\}. \quad (21)$$

Denoting $\xi(\tau) := (1 - t)R_{q(r(\tau))}^{-1}(x) + tR_{q(r(\tau))}^{-1}(y) \in T_{q(r(\tau))}\mathcal{M}$, we have

$$\begin{aligned} \delta(\tau) &= R_{q(r(\tau))}(\xi(\tau)), \\ q(r(\tau)) &= R_x(r(\tau)R_x^{-1}(y)). \end{aligned}$$

Therefore

$$\dot{\delta}(\tau) = \mathbf{D}_1 R_{q(r(\tau))}(\xi(\tau)) [(r_2 - r_1)\dot{q}(r(\tau))] + \mathbf{D}_2 R_{q(r(\tau))}(\xi(\tau)) \left[\dot{\xi}(\tau) \right],$$

with

$$\dot{q}(r(\tau)) = \mathbf{D}_2 R_{q(r(\tau))}(r(\tau)R_x^{-1}(y)) [R_x^{-1}(y)]$$

and

$$\dot{\xi}(\tau) = (1-t)\mathbf{D}_1 R_{q(r(\tau))}^{-1}(x) [(r_2 - r_1)\dot{q}(r(\tau))] + t\mathbf{D}_1 R_{q(r(\tau))}^{-1}(y) [(r_2 - r_1)\dot{q}(r(\tau))].$$

Using Proposition 21 and Lemma 14 we can bound the norms of these tangent vectors as follows:

$$\begin{aligned} \|\dot{q}(r(\tau))\|_{q(r(\tau))} &\leq L_2 \|R_x^{-1}(y)\|_x \\ &\leq L_2 M_2 d(x, y), \end{aligned}$$

$$\begin{aligned} \left\| \dot{\xi}(\tau) \right\|_{q(r(\tau))} &\leq (|1-t| + |t|) M_1 \|\dot{q}(r(\tau))\|_{q(r(\tau))} |r_1 - r_2| \\ &\leq 2M_1 L_2 M_2 d(x, y) |r_1 - r_2|, \end{aligned}$$

$$\begin{aligned} \left\| \dot{\delta}(\tau) \right\|_{\delta(\tau)} &\leq L_1 \|\dot{q}(r(\tau))\|_{q(r(\tau))} |r_1 - r_2| + L_2 \left\| \dot{\xi}(\tau) \right\|_{q(r(\tau))} \\ &\leq (L_1 L_2 M_2 + 2L_2^2 M_1 M_2) d(x, y) |r_1 - r_2|. \end{aligned}$$

Together with (21), this shows that $L_r = (L_1 L_2 + 2L_2^2 M_1) M_2$.

(iii) We define a manifold curve joining $c_r(t; x_1, y_1)$ and $c_r(t; x_2, y_2)$ as

$$\delta(\tau) = c_r(t; \delta_x(\tau), \delta_y(\tau)), \tau \in [0, 1],$$

where the curves $\delta_x(\tau) := R_{x_1}(\tau R_{x_1}^{-1}(x_2))$, $\delta_y(\tau) := R_{y_1}(\tau R_{y_1}^{-1}(y_2))$ are well-defined since endpoints belong a to retraction-convex set. Then, as previously

$$d(c_r(t; x_1, y_1), c_r(t; x_2, y_2)) \leq L(\delta) \leq \max_{\tau \in [0, 1]} \left\{ \left\| \dot{\delta}(\tau) \right\|_{\delta(\tau)} \right\}.$$

We have

$$\delta(\tau) = R_{p(\tau)}(\xi(\tau)),$$

where

$$\begin{aligned} p(\tau) &:= R_{\delta_x(\tau)}(r R_{\delta_x(\tau)}^{-1}(\delta_y(\tau))), \\ \xi(\tau) &:= (1-t)R_{p(\tau)}^{-1}(\delta_x(\tau)) + tR_{p(\tau)}^{-1}(\delta_y(\tau)). \end{aligned}$$

Differentiating these quantities with respect to τ yields

$$\begin{aligned}
\dot{\delta}(\tau) &= D_1 R_{p(\tau)}(\xi(\tau)) [\dot{p}(\tau)] + D_2 R_{p(\tau)}(\xi(\tau)) \left[\dot{\xi}(\tau) \right], \\
\dot{p}(\tau) &= D_1 R_{\delta_x(\tau)}(rR_{\delta_x(\tau)}^{-1}(\delta_y(\tau))) \left[\dot{\delta}_x(\tau) \right] + \\
&\quad D_2 R_{\delta_x(\tau)}(rR_{\delta_x(\tau)}^{-1}(\delta_y(\tau))) \left[rD_1 R_{\delta_x(\tau)}^{-1}(\delta_y(\tau)) \left[\dot{\delta}_x(\tau) \right] + \right. \\
&\quad \left. rD_2 R_{\delta_x(\tau)}^{-1}(\delta_y(\tau)) \left[\dot{\delta}_y(\tau) \right] \right], \\
\dot{\xi}(\tau) &= (1-t) \left(D_1 R_{p(\tau)}^{-1}(\delta_x(\tau)) [\dot{p}(\tau)] + D_2 R_{p(\tau)}^{-1}(\delta_x(\tau)) \left[\dot{\delta}_x(\tau) \right] \right) \\
&\quad + t \left(D_1 R_{p(\tau)}^{-1}(\delta_y(\tau)) [\dot{p}(\tau)] + D_2 R_{p(\tau)}^{-1}(\delta_y(\tau)) \left[\dot{\delta}_y(\tau) \right] \right), \\
\dot{\delta}_x(\tau) &= D_2 R_{x_1}(\tau R_{x_1}^{-1}(x_2)) \left[R_{x_1}^{-1}(x_2) \right], \\
\dot{\delta}_y(\tau) &= D_2 R_{y_1}(\tau R_{y_1}^{-1}(y_2)) \left[R_{y_1}^{-1}(y_2) \right].
\end{aligned}$$

Using Proposition 21 and Lemma 14 we establish the following bounds:

$$\begin{aligned}
\left\| \dot{\delta}_x(\tau) \right\|_{\delta(\tau)} &\leq L_2 \left\| R_{x_1}^{-1}(x_2) \right\| \leq L_2 M_2 d(x_1, x_2), \\
\left\| \dot{\delta}_y(\tau) \right\|_{\delta(\tau)} &\leq L_2 \left\| R_{y_1}^{-1}(y_2) \right\| \leq L_2 M_2 d(y_1, y_2), \\
\left\| \dot{p}(\tau) \right\|_{p(\tau)} &\leq (L_1 + L_2 M_1) \left\| \dot{\delta}_x(\tau) \right\|_{\delta_x(\tau)} + L_2 M_2 \left\| \dot{\delta}_y(\tau) \right\|_{\delta_y(\tau)}, \\
\left\| \dot{\xi}(\tau) \right\|_{p(\tau)} &\leq 2M_1 \left\| \dot{p}(\tau) \right\|_{p(\tau)} + M_2 \left\| \dot{\delta}_x(\tau) \right\|_{\delta_x(\tau)} + M_2 \left\| \dot{\delta}_y(\tau) \right\|_{\delta_y(\tau)}, \\
\left\| \dot{\delta}(\tau) \right\|_{\delta(\tau)} &\leq L_1 \left\| \dot{p}(\tau) \right\|_{p(\tau)} + L_2 \left\| \dot{\xi}(\tau) \right\|_{p(\tau)}. \tag{22}
\end{aligned}$$

By suitably plugging the previous inequalities into the right-hand side of (22), we find

$$\left\| \dot{\delta}(\tau) \right\|_{\delta(\tau)} \leq L_x d(x_1, x_2) + L_y d(y_1, y_2)$$

where L_x and L_y are polynomials of L_1, L_2, M_1 and M_2 . Then, we can take $L_{xy} = \max \{L_x, L_y\}$. \square

Corollary 25. *Let $\mathcal{U} \subset \mathcal{M}$ be any retraction-convex set as in Lemma 24. For any $x_1, x_2, y_1, y_2 \in \mathcal{U}$ and for every $r_1, r_2, t_1, t_2 \in [0, 1]$, we have*

$$\begin{aligned}
d(c_{r_1}(t_1; x_1, y_1), c_{r_2}(t_2; x_2, y_2)) &\leq (d(x_1, y_1) + d(x_2, y_2)) \left(\frac{1}{2} L_t |t_1 - t_2| + \frac{1}{2} L_r |r_1 - r_2| \right) \\
&\quad + (d(x_1, x_2) + d(y_1, y_2)) L_{xy}.
\end{aligned}$$

Proof. Using the triangular inequality and Lemma 24 we have

$$\begin{aligned}
& d(c_{r_1}(t_1; x_1, y_1), c_{r_2}(t_2; x_2, y_2)) \\
& \leq d(c_{r_1}(t_1; x_1, y_1), c_{r_1}(t_2; x_1, y_1)) + d(c_{r_1}(t_2; x_1, y_1), c_{r_2}(t_2; x_2, y_2)) \\
& \leq L_t d(x_1, y_1) |t_1 - t_2| + d(c_{r_1}(t_2; x_1, y_1), c_{r_1}(t_2; x_2, y_2)) \\
& \quad + d(c_{r_1}(t_2; x_2, y_2), c_{r_2}(t_2; x_2, y_2)) \\
& \leq L_t d(x_1, y_1) |t_1 - t_2| + L_{xy} (d(x_1, x_2) + d(y_1, y_2)) + L_r d(x_2, y_2) |r_1 - r_2|. \tag{23}
\end{aligned}$$

Exchanging (r_1, t_1, x_1, y_1) and (r_2, t_2, x_2, y_2) and repeating the same procedure leads to

$$\begin{aligned}
d(c_{r_2}(t_2; x_2, y_2), c_{r_1}(t_1; x_1, y_1)) & \leq L_t d(x_2, y_2) |t_1 - t_2| + L_{xy} (d(x_1, x_2) + d(y_1, y_2)) \\
& \quad + L_r d(x_1, y_1) |r_1 - r_2|. \tag{24}
\end{aligned}$$

Then averaging (23) and (24) proves the result. \square \square

B.2 Proof of Lemma 19

The following proof considers the RH interpolant given in Definition 5, that is with the particular choice (6) for the functions r_1, r_{01}, r_{12} , and r_{012} . Nevertheless, the result remains valid for any choice of these functions, as long as they are Lipschitz continuous.

Proof. (of Lemma 19) In the proof of Proposition 16, we show the RH interpolant H_h defined in (10) is well-defined provided $h < h_1$. In fact, then all control points to construct H_h are in contained in the retraction-convex set $B(\gamma(t), Qh) \subset B(\gamma(t), \rho_{\min})$, for some $Q > 0$ independent of h . For every $x \in \mathcal{M}$, define

$$\bar{v}(x) = \sup \left\{ v > 0 : B(x, v) \subset \mathcal{I}_x^{1/3} \right\}.$$

The constant $v_{\min} := \inf_{\tau \in [0, 1]} \bar{v}(\gamma(\tau))$ is strictly positive since, if it was zero, this would violate the Lipschitz continuity of the retraction on the compact set $\gamma([0, 1])$, guaranteed by Proposition 22. Therefore, if we require $h < h_3 := \min \left\{ h_1, \frac{v_{\min}}{2Q} \right\}$, then for any $x, y \in B(\gamma(t), Qh)$ we have

$$d(x, y) \leq d(x, \gamma(t)) + d(y, \gamma(t)) < v_{\min}.$$

Therefore, if $h < h_3$, all control points defining H_h are contained into a retraction-convex set verifying (20). Hence, in the following we can use the constants L_t, L_r and L_{xy} given by Corollary 25. Let us denote

$$p_0 = \gamma(t), \quad v_0 = \dot{\gamma}(t), \quad p_1 = \gamma(t+h), \quad v_1 = \dot{\gamma}(t+h).$$

From Corollary 7, we have that

$$H_h(\tau) = \alpha \left(\frac{\tau - t}{h}; p_0, hv_0, p_1, hv_1 \right).$$

We shall prove that there exists L_{RH} (depending explicitly on L_t, L_r and L_t) such that for any $z_1, z_2 \in [0, 1]$

$$d(\alpha(z_1; p_0, hv_0, p_1, hv_1), \alpha(z_2; p_0, hv_0, p_1, hv_1)) \leq L_{RH} h |z_1 - z_2|. \tag{25}$$

Then using (25), we can conclude that for any $\tau_1, \tau_2 \in [t, t+h]$

$$\begin{aligned} d(H_h(\tau_1), H_h(\tau_2)) &= d\left(\alpha\left(\frac{\tau_1-t}{h}; p_0, hv_0, p_1, hv_1\right), \alpha\left(\frac{\tau_2-t}{h}; p_0, hv_0, p_1, hv_1\right)\right) \\ &\leq L_{RH}h \frac{|\tau_1 - \tau_2|}{h} = L_{RH}|\tau_1 - \tau_2|. \end{aligned}$$

Let us now prove (25) by unfolding the recursive definition of α .

$$\alpha(z; p_0, hv_0, p_1, hv_1) = \beta_{012}(z, z, z) = c_z(z; \beta_{01}(z, z), \beta_{12}(z, z)).$$

Applying several times Corollary 25 we find

$$\begin{aligned} &d(c_{z_1}(z_1; \beta_{01}(z_1, z_1), \beta_{12}(z_1, z_1)), c_{z_2}(z_2; \beta_{01}(z_2, z_2), \beta_{12}(z_2, z_2))) \\ &\leq |z_1 - z_2| \frac{L_t + L_r}{2} (d(\beta_{01}(z_1, z_1), \beta_{12}(z_1, z_1)) + d(\beta_{01}(z_2, z_2), \beta_{12}(z_2, z_2))) \\ &\quad + L_{xy} (d(\beta_{01}(z_1, z_1), \beta_{01}(z_2, z_2)) + d(\beta_{12}(z_1, z_1), \beta_{12}(z_2, z_2))), \end{aligned} \quad (26)$$

$$\begin{aligned} d(\beta_{01}(z_1, z_1), \beta_{12}(z_1, z_1)) &= d(c_0(z_1, \beta_0(z_1), \beta_1(z_1)), c_1(z_1, \beta_1(z_1), \beta_2(z_1))) \\ &\leq \left(\frac{1}{2}L_r + L_{xy}\right) (d(\beta_0(z_1), \beta_1(z_1)) + d(\beta_1(z_1), \beta_2(z_1))), \end{aligned} \quad (27)$$

$$d(\beta_{01}(z_2, z_2), \beta_{12}(z_2, z_2)) \leq \left(\frac{1}{2}L_r + L_{xy}\right) (d(\beta_0(z_2), \beta_1(z_2)) + d(\beta_1(z_2), \beta_2(z_2))),$$

$$\begin{aligned} d(\beta_{01}(z_1, z_1), \beta_{01}(z_2, z_2)) &= d(c_0(z_1, \beta_0(z_1), \beta_1(z_1)), c_0(z_2, \beta_0(z_2), \beta_1(z_2))) \\ &\leq \frac{L_t}{2} |z_1 - z_2| (d(\beta_0(z_1), \beta_1(z_1)) + d(\beta_0(z_2), \beta_1(z_2))) \\ &\quad + L_{xy} (d(\beta_0(z_1), \beta_0(z_2)) + d(\beta_1(z_1), \beta_1(z_2))), \end{aligned}$$

$$\begin{aligned} d(\beta_{12}(z_1, z_1), \beta_{12}(z_2, z_2)) &\leq \frac{L_t}{2} |z_1 - z_2| (d(\beta_1(z_1), \beta_2(z_1)) + d(\beta_1(z_2), \beta_2(z_2))) \\ &\quad + L_{xy} (d(\beta_1(z_1), \beta_1(z_2)) + d(\beta_2(z_1), \beta_2(z_2))). \end{aligned} \quad (28)$$

Plugging (27)-(28) in (26) and rearranging terms yields

$$\begin{aligned} &d(c_{z_1}(z_1; \beta_{01}(z_1, z_1), \beta_{12}(z_1, z_1)), c_{z_2}(z_2; \beta_{01}(z_2, z_2), \beta_{12}(z_2, z_2))) \\ &\leq |z_1 - z_2| \frac{(L_t + L_r)(L_r + 2L_{xy}) + 2L_{xy}L_t}{4} \\ &\cdot (d(\beta_0(z_1), \beta_1(z_1)) + d(\beta_1(z_1), \beta_2(z_1)) + d(\beta_0(z_2), \beta_1(z_2)) + d(\beta_1(z_2), \beta_2(z_2))) \\ &\quad + L_{xy}^2 (d(\beta_0(z_1), \beta_0(z_2)) + 2d(\beta_1(z_1), \beta_1(z_2)) + d(\beta_2(z_1), \beta_2(z_2))). \end{aligned} \quad (29)$$

We now bound the seven distance function evaluations using once again Corollary 25.

$$\begin{aligned}
d(\beta_0(z_1), \beta_1(z_1)) &\leq \left(\frac{L_r}{4} + L_{xy}\right) (d(p_0, p_0^+) + d(p_0^+, p_1^-)), \\
d(\beta_0(z_2), \beta_1(z_2)) &\leq \left(\frac{L_r}{4} + L_{xy}\right) (d(p_0, p_0^+) + d(p_0^+, p_1^-)), \\
d(\beta_1(z_1), \beta_2(z_1)) &\leq \left(\frac{L_r}{4} + L_{xy}\right) (d(p_0^+, p_1^-) + d(p_1^-, p_1)), \\
d(\beta_1(z_2), \beta_2(z_2)) &\leq \left(\frac{L_r}{4} + L_{xy}\right) (d(p_0^+, p_1^-) + d(p_1^-, p_1)), \\
d(\beta_0(z_1), \beta_0(z_2)) &\leq L_t d(p_0, p_0^+) |z_1 - z_2|, \\
d(\beta_1(z_1), \beta_1(z_2)) &\leq L_t d(p_0^+, p_1^-) |z_1 - z_2|, \\
d(\beta_2(z_1), \beta_2(z_2)) &\leq L_t d(p_1^-, p_1) |z_1 - z_2|.
\end{aligned}$$

Inserting these bounds in (29) provides a constant $\tilde{L} > 0$ depending only on L_t , L_r and L_{xy} such that

$$\begin{aligned}
&d(\alpha(z_1; p_0, hv_0, p_1, hv_1), \alpha(z_2; p_0, hv_0, p_1, hv_1)) \\
&\leq (d(p_0, p_0^+) + d(p_0^+, p_1^-) + d(p_1^-, p_1)) \tilde{L} |z_1 - z_2|.
\end{aligned} \tag{30}$$

Using Corollary 25-(i) and denoting L_γ the Lipschitz constant of the curve γ we find

$$\begin{aligned}
d(p_0, p_0^+) &= d\left(\gamma(t), R_{\gamma(t)}\left(\frac{h}{3}\dot{\gamma}(t)\right)\right) \\
&\leq L_2 \left\| \frac{h}{3}\dot{\gamma}(t) \right\| \leq \frac{h}{3} L_2 L_\gamma, \\
d(p_1^-, p_1) &= d\left(R_{\gamma(t+h)}\left(-\frac{h}{3}\dot{\gamma}(t+h)\right), \gamma(t+h)\right) \\
&\leq L_2 \left\| \frac{h}{3}\dot{\gamma}(t+h) \right\| \leq \frac{h}{3} L_2 L_\gamma, \\
d(p_0^+, p_1^-) &\leq d(p_0^+, p_0) + d(p_0, p_1) + d(p_1, p_1^-) \\
&\leq \frac{2h}{3} L_2 L_\gamma + h L_\gamma.
\end{aligned}$$

Finally, plugging these bounds into (30) proves (25) with $L_{RH} = \tilde{L} L_\gamma \left(\frac{4}{3} L_2 + 1\right)$ and concludes the proof. \square \square